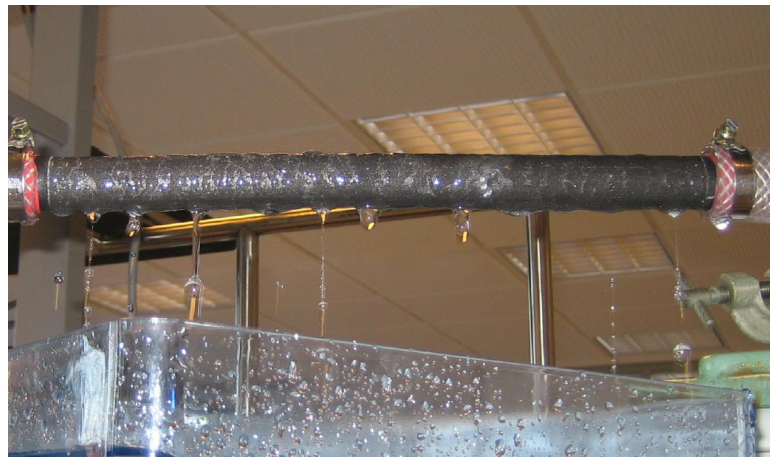Master Thesis, s011373

Flow in micro porous silicon carbide

Thomas Eilkær Hansen

Supervisor: Henrik Bruus

MIC – Department of Micro and Nanotechnology
Technical University of Denmark

March 2nd, 2007

Abstract

Flow in porous Silicon Carbide (SiC) has been investigated in order to increase the understanding of the determining parameters. Porous SiC is used in the fabrication of ceramic membranes, for use in cross-flow and dead-end filtration. Therefore, a description of the flow would help to design more efficient filtration modules, and to improve the use of the existing modules.

The investigation performed in this study consisted of preliminary calculations using the Navier-Stokes equation, and the linear Darcy's law, together with experiments. The experiments were conducted on simple SiC-components such as plugs in tubes, and porous pipes.

It was found, that the flow in porous SiC can be described with the linear Darcy's law for pore sizes around 10 μm with porosity of 45%. However, Darcy's law was found not to be applicable in the present case for porous pipes with a pore size of 10 μm and Re $\approx 10^{-4}-10^{-2}$ based on mean particle diameter. The relationship between flow rate and applied pressure was found to be above proportional, which resembles the flow behavior of a pre-Darcy region. The reason for the pre-Darcy flow is argued to be trapped air bubbles in the porous SiC, which was argued to be very dependent on the structure of the solid matrix and on the particle size distribution.

A hysteresis loop was discovered during the experiments with the porous pipe. This might verify the theory of lack of saturation, as this may be explained by the contact angle hysteresis between the air and the water due to rough surfaces of the SiC particles.

Several suggestions of recommended further experiments are stated, as the experiments conducted has been concluded to be insufficient to give a fully qualitative description of the flow in porous SiC.

Resumé

I denne afhandling er flow i porøst siliciumkarbid (SiC) blevet undersøgt, for at få en bedre forståelse for de bestemmende parametre. Porøst SiC er et keramisk materiale, der bliver brugt til fabrikation af membraner til dead-end- og cross-flow filtrering. Derfor vil en beskrivelse af flowet kunne assistere i designprocessen af disse membraner, både for at kunne producere mere effektive filtreringsmoduler, men også for at forbedre udnyttelsen af eksisterende moduler.

Undersøgelsen bestod af indledende beregninger af flowet ved at benytte Navier-Stokes' ligninger, og den lineære Darcy's lov, samt eksperimenter. Eksperimenterne bestod i at måle sammenhængende værdier for tryk og volumenstrøm igennem det porøse SiC, i to simple geometrier: En porøs blokering i et rør, samt et porøst rør af SiC.

Ud fra de fundne resultater, kan det konkluderes, at flow i porøst SiC følger den lineære Darcy's lov for middelporestørrelse omkring 10 μm med porøsitet på 45%. Dog blev det også fundet, at Darcy's lov ikke var gyldig for et porøst rør, med en middelporestørrelse på omkring 10 μm. Forholdet mellem flow hastighed og blev fundet til at være over-proportionelt, hvilket minder om pre-Darcy flow. Grunden til dette diskuteres i denne rapport, og hovedårsagen anslås til at være manglende mætning af det porøse emne, hvilket er meget afhængigt af strukturen af den porøse matrix og fordelingen af partikelstørrelser.

Der blev observeret hysterese i flowet i det porøse rør. Dette kan muligvis underbygge teorien om den manglende mætning af det porøse SiC, da en forklaring på hysteresen kan være kontaktvinkelhysterese mellem luft og vand. Dette er muligt på grund af de ru overflader af SiC-partiklerne.

Da undersøgelserne i denne rapport ikke fik de forventede resultater, vil det være nødvendigt med en mere tilbundsgående undersøgelse af de specifikke parametre i strømningerne. Derfor udmunder denne afhandling i forskellige forslag til videre arbejde.

Preface

This thesis is written between 6 June 2006 and 2 March 2007, with two months summer break, making it a total of six and a half months corresponding to 40 ECTS points.

The work of this thesis was initiated as a direct result of a student job at CoMeTas A/S, where I came in contact with SiC-membranes. The fact that this rock hard material could absorb large amounts of water intrigued the idea of making a general description of the flow in porous SiC.

The goal of the thesis was originally to end up with a full description of the flow in porous SiC, to assist in the design of ceramic cross-flow membranes. However, it soon turned out, that the flow in SiC were more complicated than anticipated, and the experiments did therefore not yield the expected results.

It should be noted that what started off as a pure micro-fluidics problem ended up with also including parts of turbulent fluid mechanics, surface and material science, thermodynamics and chemical engineering.

I would like to acknowledge CoMeTas A/S for supplying me with the SiC, and for giving me free hands to plan and design the thesis work.

Finally, I would like to express my gratitude to Henrik Bruus for extraordinary supervision, and pleasant company during the weekly discussions. Also, I would like to thank the MIFTS-group for valuable sparring during the thesis work, Tine Eilkær Hansen for illustrative assistance, Søren Beier for pleasant co-operation and help in the laboratory, everybody at CoMeTas A/S for fruitful correspondance, and finally Department of chemical engineering, especially Bente L. Jensen, for hospitality and invaluable assistance in the laboratory.

Thomas Eilkær Hansen
MIC - Department of Micro and Nanotechnology
Technical University of Denmark
2 March, 2007

Contents

List of Figures

List of Tables

List of symbols

Symbol	Description	Unit
ρ	Mass density	kg m^{-3}
$\boldsymbol{x}$	Position vector	m
w	Width of a porous wall	m
L	Length of a porous pipe	m
h	Height difference in a siphon	m
A	Area	m^2
$\mathcal{A}$	Surface area of particles	m^2
$\mathcal{V}$	Volume	m^3
$\boldsymbol{v}$	Velocity vector	m s^{-1}
v	Velocity	m s^{-1}
$\boldsymbol{g}$	Gravity	N kg^{-1}
p	Pressure	N m^{-2}
p_{tm}	Trans membrane pressure	N m^{-2}
p_{in}	Pressure at the inlet	Pa = N m^{-2}
p_{out}	Pressure at the outlet	Pa = N m^{-2}
p_{perm}	Pressure at the permeate exit	Pa = N m^{-2}
η	Dynamic viscosity	Pas = kg m^{-1} s^{-1}
Q	Volume flow rate	m^3 s^{-1}
Q_{tm}	Trans membrane volume flow rate	m^3 s^{-1}
Q_{pipe}	Volume flow rate through a pipe	m^3 s^{-1}
u	Solution to scalar problem	
k	Permeability	m^2
ϕ	Porosity	
τ	Tortuosity	
S	Surface area pr. volume of particles	m^{-1}

Chapter 1

Introduction

Filtration is an important mechanical process widely used in industries all over the world to clean up solutions of some species in a fluid. The necessity of separating mixtures, being solids and/or fluids is applied in both households, e.g. in the making of coffee and in vacuum cleaners, as well as in large industries, such as the cleaning of waste water and separation of yeast from beer. There are two major types of filtration: dead-end filtration and cross-flow filtration, as sketched in Fig. 1.1.
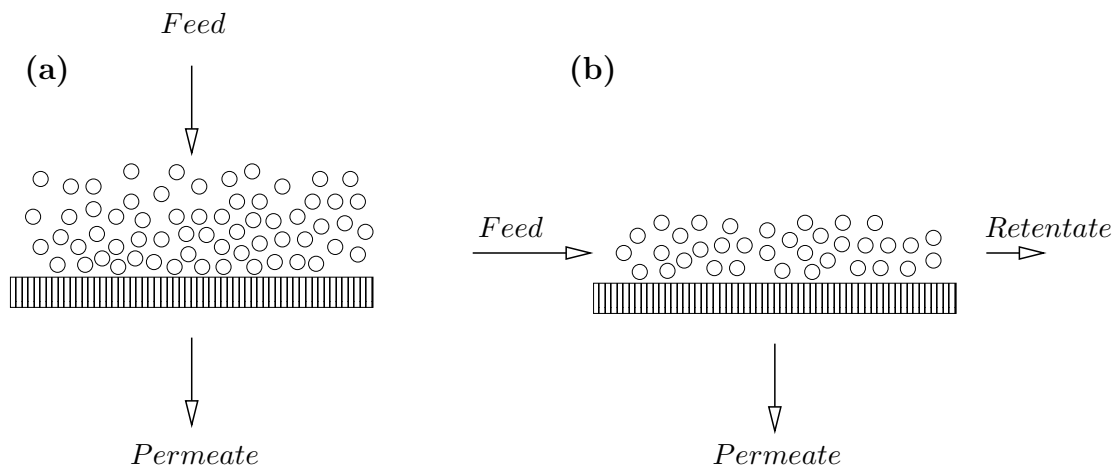
Figure 1.1: *Principles of dead-end and cross-flow filtration.(a) All of the fluid to be filtered passes through the membrane and all particles larger than the pore size are retained at the surface of the membrane. This results in a "filter cake" as the trapped particles start to build up.(b) The medium to be filtered flows through the open channels of the membrane carrier, which result in particles being retained in the channel flow if their size exceeds the radius of the membranes pores, building up the concentrate. The permeate flows by cross-flow through the pores. Notice the retentate flow of the cross-flow filtration, which removes the retained media and thereby prevents fouling.*

Dead-end filtration is an energy efficient method, but it is troubled by fouling of the filter during use, a well-known example being a used vacuum cleaner bag. Cross-flow filtration is less energy efficient, but is less exposed to fouling. This is due to the flow in the open channel of the contaminated fluid, containing a higher concentration of the solid residue known as retentate.

1.1 Background of the thesis work

CoMeTas A/S is a company situated at Scion, DTU. It has a production facility with ceramic membranes in porous silicon carbide (SiC) as one of its main products. These membranes can be used in dead-end, as well as in cross-flow filtration.

CoMeTas A/S is founded February 2006, therefore CoMeTas and its products are fairly new. The exact knowledge of flow in ceramic membranes is therefore limited. This, combined with the fact that SiC differs from other ceramic materials in the sense of its chemical, and material properties, constitutes the background for this thesis work.

1.2 Membranes and silicon carbide

In simple practical terms, a membrane can be defined as a semipermeable active or passive barrier, which, by the action of a certain driving force, permits preferential passage of one or more selected species or components (molecules, particles or polymers) of a fluid or solution, Ref. [7]. In a ceramic membrane, the passive barrier is constructed as small particles of ceramic material sintered together, where the size of the particles, and the way they are sintered together, are significant for the specifications of the membrane. Advantages of ceramic membranes compared to other materials are their high flux, their high chemical and physical stability, their well defined separation characteristics and their long working life. Disadvantages are the weight and the considerable production costs of ceramic components. However, the latter are generally compensated for by a long service life-time, Ref. [9].

A typical membrane from CoMeTas A/S is constructed by having a carrier of larger particles, coated with one or more layers of smaller particles, the outermost being the membrane layer. This construction increases the flow rate through the porous SiC compared to a porous medium consisting solely of membrane layer-sized particles, as the membrane layer has a significant higher resistance than the carrier. The carrier and membrane are both solely made of porous SiC. SiC is a ceramic compound of silicon and carbon, which is highly inert chemically and has a low thermal expansion coefficient compared to metal. It is one of the hardest known materials, which reduces the wear of the membrane. SiC is also generally considered to yield a higher flow rate as a function of the pressure compared to other ceramic materials. These structural and chemical characteristics are all appreciated in a material for membranes, as they expand the area of use to almost any industry.

The sintering process of SiC is performed by heating a clay, consisting of SiC particles and a dispersion media. As the mixture is heated, the dispersion media vanishes, and the smaller particles vaporize, and instantly crystallize again on the surfaces of larger particles,

causing a "weld" of the particles. The structure can be seen on the picture in Fig. 1.2. This manufacturing method means that the completed membrane unit will have a particle
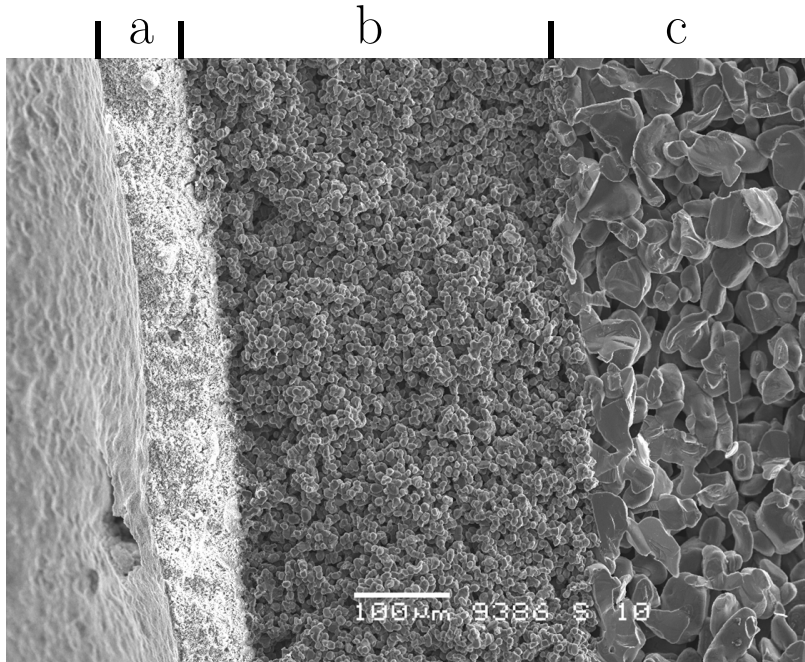
Figure 1.2: *SEM-picture showing the structure of SiC particles sintered together by smaller particles. The picture shows three layers: (a) is the membrane coating, (b) is an intermediate layer, and (c) is the carrier.*

size distribution and not a fixed particle size. As the particles also vary in shape, the properties of a given membrane are characterized by the pore sizes. This also makes it easier to predict the ability to filter a given solution.

SiC-membranes are in particular useful in ultra- and microfiltration. The pore size for ultrafiltration and microfiltration is below 0.1 μm, and from 0.1 μm to 10 μm, respectively.

1.3 Problem formulation

The goal of this thesis is to investigate and characterize liquid flow through porous SiC-membranes. This investigation is carried out theoretically, by calculating the flow parameters using analytic models and by numerical simulation using the software COMSOL Ref. [10], and experimentally, by testing the results in various test setups. The porous SiC is provided by CoMeTas A/S in various forms.

The focus of the thesis work will be the actual flow phenomena in the SiC, and not the filtration process.

1.4   Thesis work history

The thesis work started 6 June, 2006, by a three-week literature study, and a general introduction to filtration and flow in porous media as my knowledge of porous media was very limited prior to the thesis work. After a two-months summer break, the theoretical calculations, and planning of experiments commenced 4 September 2006.

The area of flow investigation in cross-flow SiC-membranes has not been investigated at DTU prior to this thesis work, which necessitated a thorough review of existing relevant knowledge and experimental equipment. As the flow in porous SiC is at micro scale, the thesis work was conducted at Department of Micro and Nanotechnology (MIC) in the Microfluidics Theory and Simulations Group, under supervision of Prof. Henrik Bruus. However, as MIC had no prior experience with porous media flow, the experimental work was conducted at Department of Chemical Engineering, by the courtesy of prof. Gunnar Jonsson and PhD - student Søren Beier.

To assist with the theoretical background, Prof. Philip Binning from Department of Environment & Resources was consulted for general knowledge concerning flow in porous media. Jens Nørkjær from Department of Mechanical Engineering has been consulted for fluid mechanics in large scale, and finally the workshop at Department of Physics for experimental equipment.

In the final weeks of the thesis work, it was drawn to my attention that Assoc. Prof. Alexander Shapiro, Department of Chemical Engineering at DTU, is an expert in gas flow in porous media. He was consulted, and was helpful as a sparring partner by clarifying some issues when writing the thesis.

1.5   The structure of the thesis

- Chapter 2: To investigate the flow in SiC, it is important to know the flow regime. Therefore, this chapter concerns with the governing equations to be used, and general model considerations, including COMSOL simulations.

- Chapter 3: This chapter contains the theoretical background for conducting the experiments. The chapter is divided into two parts, 1D and 2D considerations.

- Chapter 4: The experimental set-ups are described in this chapter, including fabrication of the SiC. It also contains a discussion of challenges encountered in the process of conducting the experiments.

- Chapter 5: The initial experiment is called "plug-flow". The results and a discussion of the results are presented in this chapter.

- Chapter 6: The first experiments in two dimensions were conducted as the "open-pipe cross-flow" experiments, with a primary flow in the pipe. The results of these, followed by a discussion, are presented in this chapter.

- Chapter 7: This chapter describes the experiments conducted with the second, and final, two-dimensional experimental set-up, the so-called "blocked-pipe cross-flow"

experiments. These experiments consisted of two different ways of applying the pressure in the pipe, hydro static pressure and a regular pump.

- Chapter 8: This chapter collects the results from the experiments, and attempts to explain the observed flow phenomena. Suggestions of further investigations are described.

- Chapter 9: The combined results of the theoretical calculations, and the experiments are summarized and discussed in this chapter. To complete a full analysis of flow in porous SiC, additional work is needed, which also is described in this concluding chapter.

Chapter 2

Model Considerations

The goal of this project was to investigate flow in porous SiC for applications in cross-flow membrane filtering. However, as the flow in porous SiC in the vast majority of cases will be combined with a free fluid flow, e.g. a channel flow or a pipe flow, two flow situations must be considered: flow in the porous medium and regular fluid flow in open channels.

2.1 General fluid mechanics

The flow in the open channels of a membrane carrier follows standard fluid mechanics theory, where conservation of linear momentum is given by the Navier-Stokes equation, based on Newton's second law. For incompressible fluids it yields

$$\rho\left[\partial_t \mathbf{u} + (\mathbf{u} \cdot \boldsymbol{\nabla})\mathbf{u}\right] = -\boldsymbol{\nabla} p + \eta \nabla^2 \mathbf{u} + \rho \mathbf{g}. \tag{2.1}$$

The terms on the left-hand-side of the equation are the inertial forces, and the right-hand-side consists of the pressure gradient and the viscous forces. The term $\rho\mathbf{g}$ regarding the influence of gravity is neglected throughout this thesis.

It turns out to be convenient to non-dimensionalize Eq. (2.1) by using following dimensionless variables based on d_0, a typical length scale, and V_0 a characteristic velocity of the flow

$$\mathbf{r} = d_0 \tilde{\mathbf{r}}, \tag{2.2a}$$

$$\mathbf{u} = V_0 \tilde{\mathbf{u}}, \tag{2.2b}$$

$$t = \frac{d_0}{V_0}\tilde{t}, \tag{2.2c}$$

$$p = \frac{\eta V_0}{d_0}. \tag{2.2d}$$

Inserting Eq. (2.2) into Eq. (2.1) results in

$$\mathrm{Re}\left(\tilde{\partial}_t \tilde{\mathbf{u}} + (\tilde{\mathbf{u}} \cdot \tilde{\boldsymbol{\nabla}})\tilde{\mathbf{u}}\right) = -\tilde{\boldsymbol{\nabla}}\tilde{p} + \tilde{\nabla}^2 \tilde{\mathbf{u}}, \tag{2.3}$$

where the tilde indicates the non-dimensional form, and where the dimensionless parameter
Re, the Reynolds number, appears naturally as

$$\text{Re} = \frac{\rho V_0 d_0}{\eta}. \tag{2.4}$$

If Re is low, the viscous forces are predominant, which means that the inertial forces can
be neglected. In that case the flow is laminar, and Eq. (2.3) becomes

$$\tilde{\boldsymbol{\nabla}}\tilde{p} = \tilde{\nabla}^2\tilde{\mathbf{u}}, \tag{2.5}$$

which is called the Stokes equation.

If Re is high, the laminar flow will break down and become unstable, and the inertial
forces will then dominate the flow. If Re becomes sufficiently high, the flow will evolve
into a new flow regime which is fully turbulent, Ref. [5].

Turbulence has following characteristics:

- Temporal and spatial fluctuations in pressure and velocity. The velocity will fluctuate
  in three dimensions.

- Eddies in various sizes will form.

- Self-sustaining motion. Especially in wall-bounded flows, the turbulent flow can
  sustain itself by producing new eddies to replace those lost by viscous dissipation.
  Eddies are produced by the shear stress from the wall, and in the fluid.

- Mixing is much stronger in a turbulent flow than that of a laminar flow, as the
  turbulent eddies move about in three dimensions.

The velocity and the pressure in a turbulent regime is normally described by time-
averaging:

$$\bar{\mathbf{u}} = \frac{1}{T} \int_{t_0}^{t_0+T} \mathbf{u}\, dt, \quad \bar{p} = \frac{1}{T} \int_{t_0}^{t_0+T} p\, dt, \tag{2.6}$$

where T is larger than any significant time period of the fluctuations in u. The velocity
and pressure in the flow can then be defined as

$$\mathbf{u} = \mathbf{u}' + \bar{\mathbf{u}}, \tag{2.7a}$$

$$p = p' + \bar{p}, \tag{2.7b}$$

where $\mathbf{u}'$ and p' are the fluctuation terms. By inserting these into Eq. (2.1), the Navier-
Stokes equation for turbulent fluid flow becomes, using Einstein notation for convenience

$$\rho\big[\partial_t \bar{u}_i + \bar{u}_j \partial_j \bar{u}_i\big] + \rho\, \partial_j\left(\overline{u_i' u_j'}\right) = -\partial_j \bar{p} + \eta\, \partial_j^2 \bar{u}_i. \tag{2.8}$$

By rewriting Eq. (2.8) to the energy equation for the flow, it is obtained that turbulence
extracts energy from the main flow at a rate of $\dot{E}$ given by

$$\dot{E} = (-\rho\overline{u_i' u_j'})\partial_i x_j. \tag{2.9}$$

From the result above it can be seen that turbulence is generated near the wall of the flow, as the velocity gradient is largest there due to the no-slip condition.

The energy flux $\dot{E}$ will not be calculated, as it will involve complex numerical calculations, which is outside the scope for this thesis work. It is only stated to give an impression of the important parameters for the production of turbulence.

2.2 Flow in porous media

A porous medium is defined as a volume, consisting of a solid permeated by pores filled with a fluid, being liquid or gas. The solid is referred to as "*the solid matrix*", whereas the space filled with fluid is "*the void space*". At least some of the pores should be interconnected, to make the volume permeable, cf. Ref. [1].

2.2.1 Solid matrix structure and permeability

The picture in Fig. 2.1 shows the solid matrix of the SiC. The complexity of the matrix makes it an almost impossible task to describe the geometry in an exact manner. However, it does, combined with the fact that the pores are in the micrometer scale, make it possible and advantageous to describe the porous medium as a continuum, where the hydraulic resistance in each pore is averaged to a hydraulic resistance of the medium.

This resistance is dependent on both fluid properties and on the properties of the solid matrix of the medium. In analogy to Ohm's law in electrical theory, the conductivity is defined as the inverse of the resistance.
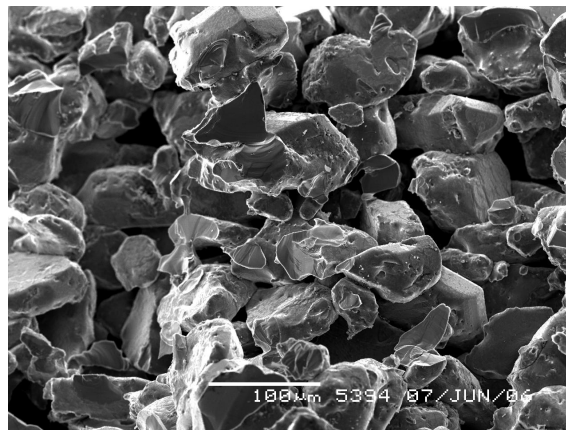
Figure 2.1: *SEM-picture of the solid matrix. Observe the variations in particle shape and size.*

The hydraulic conductivity of a porous medium is denoted the permeability k with unit [m^2], and it is typically used to provide an indication of the capacity of a porous medium for allowing fluid to penetrate; a high permeability means a high throughput.

There are three macroscopic properties, which rely to the permeability in a consolidated medium. The first is the porosity defined as the ratio of the volume of the void space in

the medium, $\mathcal{V}_{\text{void}}$ and the total volume of the medium $\mathcal{V}_{\text{total}}$

$$\phi = \frac{\mathcal{V}_{\text{void}}}{\mathcal{V}_{\text{total}}} \tag{2.10}$$

It should be noted that there are two types of void space which can be used to calculate the porosity: Effective void space and isolated void space, Ref. [2]. The isolated pore space are the blind pores, which are either only interconnected from one side or not at all. As seen on Fig. 2.1, SiC is very porous, and it is assumed that it does not contain any significant blind pores.

The second property regarding the permeability is the surface area of the particles $\mathcal{A}$, pr. total volume

$$S = \frac{\mathcal{A}}{\mathcal{V}_{\text{total}}}. \tag{2.11}$$

Assuming spherical particles, with d_m being the mean diameter of the particles, S can be described as

$$S = \frac{6}{d_m}. \tag{2.12}$$

The third property is tortuosity and is based on the fact that the flow path of the fluid in the porous medium is very complicated, or "tortuous". Using w as the direct distance between inlet and outlet, and w_e as the length of the actual flow path, the tortuosity is defined as

$$\tau = \left(\frac{w}{w_e}\right)^2. \tag{2.13}$$

The hydraulic diameter d_h is a commonly used term when flow in noncircular tubes and channels are calculated. Using this term, it is possible to calculate the parameters for a flow, assuming a round tube. A similar hydraulic diameter can be defined in a porous medium as

$$d_h = 4\frac{\phi}{S(1-\phi)}, \tag{2.14}$$

for a set of capillaries. This is used to define Eq. (2.15) as the basic form of an equation to calculate permeability, Ref. [19], by assuming that the porous medium can be described by a set small capillaries

$$k = \frac{\phi}{16}\frac{\tau}{c_0}d_h^2, \tag{2.15}$$

where c_0 is a dimensionless shape factor of the capillaries. The shape factor is introduced to compensate for the non-circular shape of the pores. c_0 is proposed to be in the range of 2.5 - 3.0, Ref. [1]. Inserting the hydraulic diameter in Eq. (2.15) yields

$$k = \frac{\phi^3}{S^2(1-\phi)^2}\frac{\tau}{c_0}, \tag{2.16}$$

also known as the *Kozeny-Carman* equation. Using a value of $c_0 = 2.5$ and a tortuosity of $\tau = 0.5$, assuming $w_e = \sqrt{2}w$, following equation is obtained,

$$k \quad = \quad \frac{d_m^2}{180} \frac{(1-\phi)^2}{\phi^3}, \tag{2.17}$$

assuming spherical particles.

This equation can be used to estimate the permeability of a given porous medium, using properties as the porosity and the mean particle size, which are generally known for a porous medium. It is important to emphasize that Eq. (2.17) is based on empirical data, and should therefore only be used to get an estimate of the permeability. To get an exact value, it is necessary to conduct flow experiments. The permeability normally ranges from 10^{-7} m^2 in very pervious materials, such as clean gravel, to 10^{-20} m^2 in materials, which are almost impervious, such as concrete.

2.2.2 Flow regions and governing equations

When applying the continuum approach to the porous matrix, the flow in porous media can be divided into four regions on phenomenological ground: pre-Darcy flow, Darcy flow, Forchheimer flow and turbulent flow. Darcy flow means that it is governed by the linear Darcy's law. The transitions between these regions are smooth, which means that it is difficult to determine the flow in the transition zones. Fig. 2.2 shows the general relationship between each region.

The demarcation parameter between the regions is typically the Reynolds number, Eq. (2.4), based on the mean grain diameter. Ref. [16] states that Darcy flow occurs at Re $_{DL}$ < Re $\leq$ 2.3, where Re $_{DL}$ is the lower limit for Darcy flow, and is below 10^{-5} in simple media, i.e. the particles can be characterized as spheres. At $5 <$ Re < 80 the flow can be characterized as Forchheimer flow, and at Re > 120 the flow is fully turbulent, i.e. viscous forces can be neglected. It is important to emphasize that the values of the demarcation parameter stated here are the results of the work from a single reference, Ref. [16]. As there are a general agreement on the existence of the four flow regions, e.g., Ref. [18] and Ref. [17], the values are subject to disagreement in the porous media flow community.

Pre-Darcy flow is governed by molecular effects, and is thus dependent on the individual flow parameters. There does not exist a generally accepted theory for describing this flow region.

Darcy flow, on the other hand, can be described by Darcy's law, Eq. (2.18), which is an expression of conservation of momentum. It describes a linearity between flow rate and applied pressure and is similar to Ohm's law in electricity, and Fourier's law in heat conduction. Darcy's law is developed experimentally by Darcy in 1856, by using a sand filter, however, Darcy's law can also be derived from a spatial average of Stoke's equation, Eq. (2.5), Ref. [12], to

$$\boldsymbol{\nabla} p = \frac{16}{\phi} \frac{c_0}{\tau} \frac{\eta}{d_h^2} \mathbf{v} = \frac{\eta}{k} \mathbf{v}, \tag{2.18}$$

where $\mathbf{v}$ is the macroscopic velocity defined as $\mathbf{v} = \mathbf{Q}/A$, and k the permeability defined in the previous section.
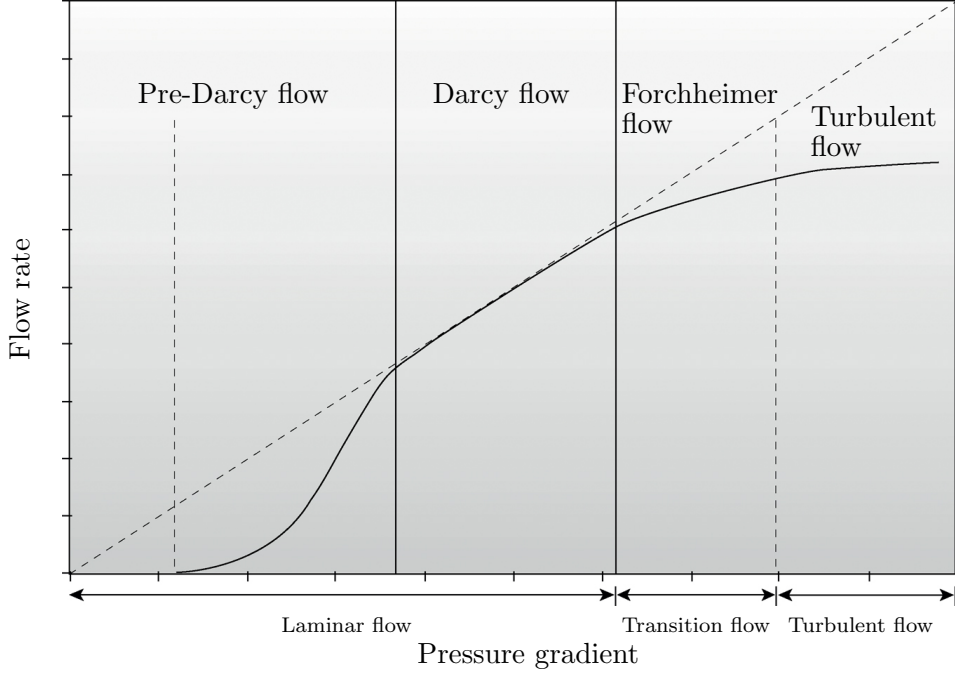
Figure 2.2: *Graph of relationship between the regions of the flow. Pre-Darcy flow and regular Darcy flow occurs in the laminar region, the transition between laminar and turbulent flow is called the Forchheimer flow, and finally the fully turbulent region, where viscous forces are neglected.*

In membrane technology it is standard to assume validity of Darcy's law. The focus of the calculations and the experiments in this thesis work will therefore be to confirm or to falsify this assumption.

The following assumptions has to be valid to apply Darcy's law:

1. Inertia can be neglected, as the theoretical derivation of Eq. (2.18) originates in laminar flow theory.

2. Constant pressure drop in the SiC.

3. Isotropic medium is assumed, as the grains in SiC are uniformly distributed. If the medium is anisotropic, the permeability will vary in space.

4. Heterogeneous fluid, i.e. constant density

5. Saturated flow, i.e. single fluid flow.

Assuming 1D-flow and a linear pressure distribution, Darcy's law becomes

$$v = \frac{\eta}{k}\frac{\Delta P}{w}, \tag{2.19}$$

where ΔP is the pressure difference across the membrane, and w is width of the membrane.

When inertial effects starts to influence the flow, Darcy's law is no longer applicable. This is due to the initiation of turbulence in the flow, as described in Section 2.1. When turbulence occur, eddies will be generated, which energy from the main flow. Eq. (2.20) is Forchheimer's equation, and is an extension of Darcy's law, to describe the flow in this region. The energy extracted by the turbulence is converted to kinetic energy of the eddies, therefore an extra term is added to Darcy's law, $\rho\mathbf{v}^2$ in the flow:

$$\boldsymbol{\nabla} p = \frac{\eta}{k}\mathbf{v} + \beta\rho\mathbf{v}^2, \tag{2.20}$$

where β is the Forchheimer number, with the unit $[m^{-1}]$, which is deduced experimentally.

When the flow is fully turbulent, viscous forces are ignored. The flow is unstable and unsteady, which necessitates the use of statistical methods to describe the flow.

2.2.3 Brinkman extension

As mentioned in the introduction to this chapter, the flow in a membrane consists of two domains. At the interface between these domains, an extension to Darcy's law is needed, which is the Brinkman equation

$$\boldsymbol{\nabla} p = -\frac{\eta}{k}\mathbf{v} + \eta\nabla^2\mathbf{v}. \tag{2.21}$$

The Brinkman equation will be studied in Chapter 3.

2.2.4 Example

To determine whether or not it is reasonable to assume Darcy flow in a SiC-membrane from CoMeTas A/S, an estimate of the Reynolds number is made. In a typical membrane, the wall thickness is $w \approx 3 \times 10^{-3}$ m. The pressure difference across the membrane is called the trans membrane pressure, p_{tm}, with a typical value of $p_{\text{tm}} \approx 3 \times 10^5$ Pa. Using a porosity of $\phi = 0.45$ of the SiC and an average particle size of $d_m = 10 \times 10^{-6}$ m, the permeability can be calculated to $k = 1.67 \times 10^{-13}$ m^2 using Eq. (2.17). With water at 20 °C as fluid, the viscosity is $\eta = 10^{-3}$ Pa s which by Eq. (2.19) yields a velocity of

$$v = 0.02 \ \frac{\text{m}}{\text{s}} \tag{2.22}$$

The Reynolds number calculated from Eq. (2.22) is Re = 0.17 using Eq. (2.4) and $\rho = 998$ kg/m^3 for water. As this number is below 2.3, the limit for Darcy flow (see Section 2.2.2), it is concluded so far that Darcy's law should be applicable in the present set-up. However, it will still be possible to change other parameters, e.g., the particle size. The table below shows calculations of Reynolds number, using different particle sizes and different trans membrane pressures.

From the calculations of the Reynolds number in Table 2.1, it can be concluded that these preliminary calculations indicate Darcy flow in the SiC membranes.

d_m [μm]	ΔP[Pa]	Re
6×10^{-6}	1×10^5	0.01
6×10^{-6}	3×10^5	0.04
10×10^{-6}	1×10^5	0.06
10×10^{-6}	3×10^5	0.17
21×10^{-6}	1×10^5	0.52
21×10^{-6}	3×10^5	1.55

Table 2.1: Predicted values of Reynolds number. The mean diameters are taken from Ref. [11]

Chapter 3

Model Calculations

This chapter contains the theoretical basis of this thesis. The governing equations are studied, and different values of the flow parameters are tested.

In 1D, the application of Darcy's law in porous SiC plugs will be tested. This is done by assuming laminar flow, and then applying laminar flow theory.

In 2D, the pressure inside a porous tube is investigated. As fluid penetrates the pipe, the pressure inside the pipe will drop. This pressure drop is investigated, as it may have a significant importance to the flow velocity in the porous SiC throughout the pipe.

The calculations of the model is divided into 1D and 2D considerations.

3.1 1D model of flow through SiC

In Chapter 2 it was assumed, on the base of literature studies and preliminary calculations, that Darcy's law was applicable in the present situation. It will now be investigated, what influence the dissipation, which was introduced in Brinkman's equation Eq. (2.21), has on the results.

3.1.1 Analytical solution of the 1D model

The initial step in finding the governing equations for the flow in porous silicon carbide, is to set up a simple flow problem in a pipe, with a plug of silicon carbide, as seen in Fig. 3.1. The flow in the pipe is assumed laminar, and can therefore be described as a Poiseuille-Darcy flow, i.e. Poiseuille flow in the pipe, and Darcy flow in the porous medium. The Poiseuille-Darcy flow follows the Brinkman equation, which is Stokes equation extended with a dissipative force against the flow

$$0 = -\boldsymbol{\nabla} p + \eta \nabla^2 \mathbf{v} - \alpha \mathbf{v}. \tag{3.1}$$

As the dissipative term originates in the porous medium, α is chosen to $\alpha = \frac{\eta}{k}$. Outside the porous medium, $\alpha = 0$, where k is the permeability.
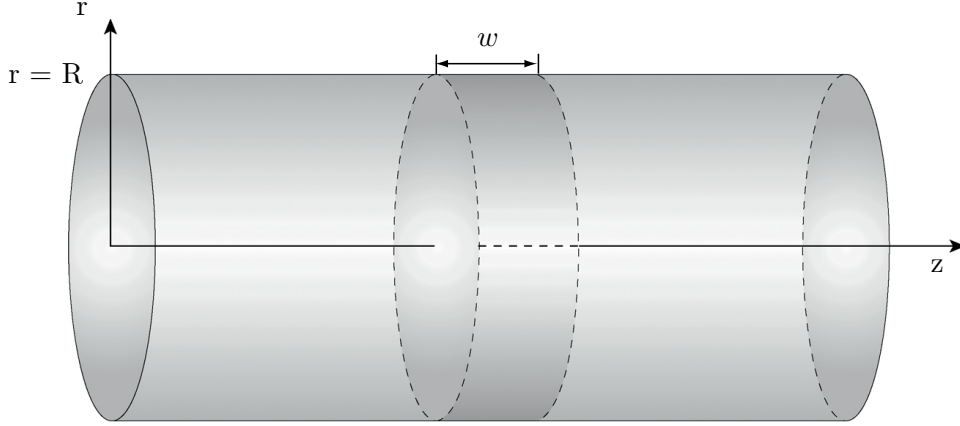
Figure 3.1: *Plug of SiC in a pipe. The radius of the pipe is R, which is the same radius as the plug. The length of the plug is denoted w*

With the assumption of a constant pressure drop in the porous medium, i.e. $\boldsymbol{\nabla} p = -\frac{\Delta p}{w}$, Eq. (3.1) becomes

$$\frac{1}{r}\partial_r v_x + \partial_r^2 v_x = \frac{1}{k}v_x - \frac{1}{\eta}\frac{\Delta p}{w}, \tag{3.2}$$

using cylindrical coordinates. This is non-dimensionalized by the length scale $\ell = \sqrt{k}$, and the velocity $v_0 = \frac{k}{\eta}\frac{\Delta p}{w}$, using the non-dimensional parameters $s = r/\ell$, $\tilde{s} = R/\ell$ and $u(s) = v_x(r)/v_0$ to

$$u''(s) + \frac{1}{s}u'(s) - u(s) + 1 = 0. \tag{3.3}$$

The solution of the above is given by a particular solution, u_p, and a solution to the homogeneous equation, u_p, i.e.

$$u(s) = u_h(s) + u_p(s). \tag{3.4}$$

A particular solution is easily seen to be $u_p(s) = 1$. The homogeneous equation is recognized as the modified Bessel equation of zeroth order, yielding a solution of the kind

$$u_h(s) = C_2 I_0(s) + C_1 K_0(s), \tag{3.5}$$

which gives a total solution of

$$u(s) = C_2 I_0(s) + C_1 K_0(s) + 1. \tag{3.6}$$

The boundary conditions are $u(\tilde{s}) = 0$ (no-slip) and $\partial_r u(r) = 0|_{r=0}$ (due to symmetry). As $\partial_r K_0$ diverges for $r \to 0$ because of the logarithmic part, C_1 must be zero. The no-slip condition yields $C_2 = -1/I_0(\tilde{s})$, and therefore the solution becomes:

$$u(s) = 1 - \frac{I_0(s)}{I_0(\tilde{s})}. \tag{3.7}$$

This problem is studied in the two limits, $\tilde{s} \ll 1$, and $\tilde{s} \gg 1$.

In the limit $\tilde{s} \ll 1$, i.e. $R \ll \sqrt{k}$, the solution can be expanded utilizing the series

$$I_0(s) = \sum_{n=0}^{\infty} \frac{1}{(2^n n!)^2} s^{2n} = 1 + \frac{1}{2^2} s^2 + \frac{1}{2^2 4^2} s^4 + \frac{1}{2^2 4^2 6^2} s^6 + \dots \tag{3.8}$$

If $\tilde{s} \ll 1$ in Eq. (3.7), then

$$u(s) = \frac{1}{4}(\tilde{s}^2 - s^2). \tag{3.9}$$

With the insertion of the specific length and velocity, this solution becomes

$$v_x(r) = \frac{1}{4\eta} \frac{\Delta p}{w} (R^2 - r^2), \quad \text{for } R \ll \sqrt{k}, \tag{3.10}$$

which is the Poiseuille pipe-flow solution for laminar flow. This result was expected, because if the permeability k is large, the material will not give any significant resistance to the flow, and therefore, the flow will behave like there were no porous material at all.

In the present case, using the permeability calculated in Section 2.2.4, the data from silicon carbide is $\ell \approx 4.0 \times 10^{-7}$ m, and a radius of R $= 0.8 \times 10^{-3}$ m. This indicates $\tilde{s} \approx 2.0 \times 10^4$, which is several orders of magnitudes larger than 1.

In the limit $\tilde{s} \gg 1$, i.e. $R \gg \sqrt{k}$, I_0 has the asymptotic form

$$I_0(s) = \frac{1}{\sqrt{2\pi s}} e^s, \tag{3.11}$$

which becomes

$$u(s) = \begin{cases} 1 & \text{for } s > 10^{-4}\tilde{s}, \\ 1 - \sqrt{\frac{\tilde{s}}{s}} e^{-(\tilde{s}-s)} & \text{for } s < 10^{-4}\tilde{s}, \end{cases} \tag{3.12}$$

when inserted into Eq. (3.7). The deviation from unity close to the wall at $s = 10^{-4} \tilde{s}$, which corresponds to a distance of 1×10^{-6} m from the wall, is only 0.7% and it is therefore a good approximation to use $u(s) \equiv 1$. The velocity will thus be constant with the value

$$v_x(r) = v_0 = \frac{k}{\eta} \frac{\Delta p}{w}, \quad \text{for } R \gg \sqrt{k}. \tag{3.13}$$

This is recognized as Darcy's law. It can therefore be concluded that the flow in the plug can be approximated by the linear Darcy's law.

The expected relation between flow rate Q_{tm}, and the pressure difference Δp is plotted in Fig. 3.2. If indeed Darcy's law is applicable in porous SiC, the experiments should produce a graph similar to this.
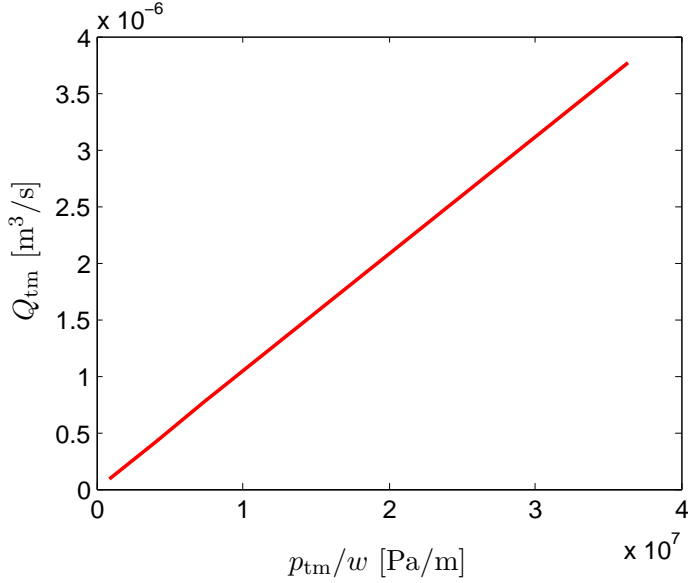
Figure 3.2: *The expected flowrate through the plug, Q_{tm}, as a function of the pressure gradient. The permeability, $k = 1.7 \times 10^{-13}$ is calculated from Eq. (2.16), using $\phi = 0.45$ and $d_m = 12\ \mu m$.*

3.1.2 COMSOL

A simple model of the plug in a pipe has been analyzed using in COMSOL[1] to verify the analytical calculations from the previous section. The resulting velocity field is shown in Fig. 3.3. The flow field is calculated in a 2D domain, using axial symmetry.

By calculating the flow for different plug lengths, it was possible to determine the relationship between the length of the plug and the flow rate. Fig. 3.4 shows the expected flow rate as a function of $1/L$. It is concluded that the COMSOL simulations confirm the analytical calculations in the previous section, and therefore Darcy's law should be valid.

3.2 2D Analytical model

An effective cross-flow membrane is characterized by a high flux and good filtration abilities. Both are dependent on the pressure drop through the channel, which will be discussed in this section. A sketch of the flow is seen in Fig. 3.5.

---

[1]All calculations in COMSOL is done in the multiphysics package, assuming axial symmetry in 2D. The flow is assumed to be steady state, and the fluid incompressible.
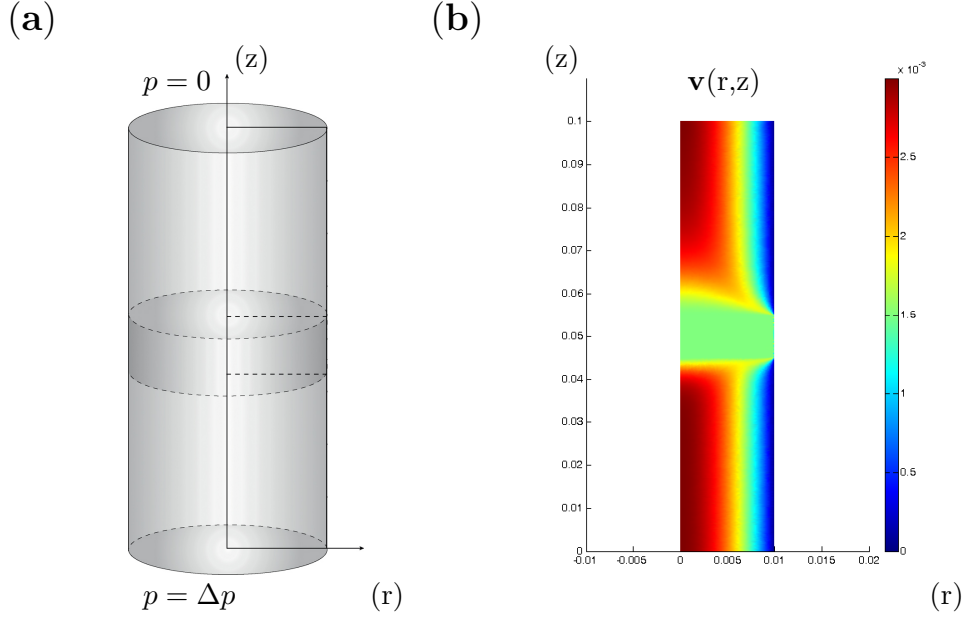
Figure 3.3: *(a) A sketch of the model simulated in COMSOL. (b) A color plot of the velocity field in the (r,z) plane calculated in COMSOL, where the red color indicates high velocity, and blue indicates low. The velocity field is seen to be homogeneous in the plug, as predicted by the analytical calculations.*

3.2.1 Laminar flow in the pipe

In this section, it is assumed that the flow in the pipe is laminar, and that Darcy's law is valid. Due to mass conservation, the relation in a slice of length dx between incoming pipe flow rate $Q_{\text{pipe}}(x)$, the outgoing pipe flow rate $Q_{\text{pipe}}(x + dx)$ and Q_{tm} through the permeable wall is

$$Q_{\text{pipe}}(x) = Q_{\text{pipe}}(x + dx) + Q_{\text{tm}}(x)dx, \tag{3.14}$$

where subscript tm is for trans membrane. The flow in the infinitesimal piece, dx long, is assumed to be a Poiseuille flow

$$Q_{\text{pipe}}(x) = \frac{\pi R^4}{8\eta}p'(x). \tag{3.15}$$

It was showed in Section 3.1 that the flow in porous SiC could be described by the linear Darcy's law,

$$Q_{\text{tm}} = \frac{2\pi Rk}{\eta w}\Delta p(xd)dx, \tag{3.16}$$
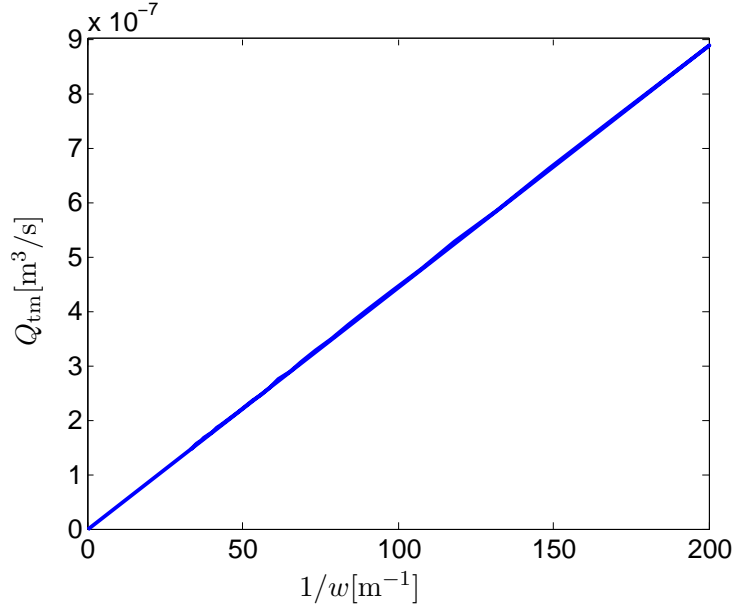
Figure 3.4: *The expected flow rate through a plug as a function of 1/w, with w being the length of the plug. Other flow parameters are $\Delta p = 10^5 Pa$, permeability $k = 3.0 \times 10^{-13} m^2$, radius of plug $R = 10^{-2} m$, density for water $\rho = 1000 kg/m^3$ and viscosity for water $\eta = 10^{-3} Pa\, s$*

which, when inserted into Eq. (3.14) together with Eq. (3.15), yields

$$-\frac{\pi R^4}{8\eta} p'(x) = \frac{k}{\eta w} \Delta p 2\pi r dx - \frac{\pi R^4}{8\eta} p'(x + dx). \tag{3.17}$$

As $\frac{p'(x+dx)-p'(x)}{dx} \approx p''(x)$, Eq. (3.17) becomes

$$p''(x) = \lambda^2 \Delta p(x) \tag{3.18}$$

using $\Delta p = p(x) - p_{\mathrm{perm}}$. The constant λ is given by

$$\lambda = \sqrt{\frac{16k}{wR^3}}. \tag{3.19}$$

Setting $p_{\mathrm{perm}} = 0$, the solution is

$$p(x) = Ae^{\lambda x} + Be^{-\lambda x}. \tag{3.20}$$
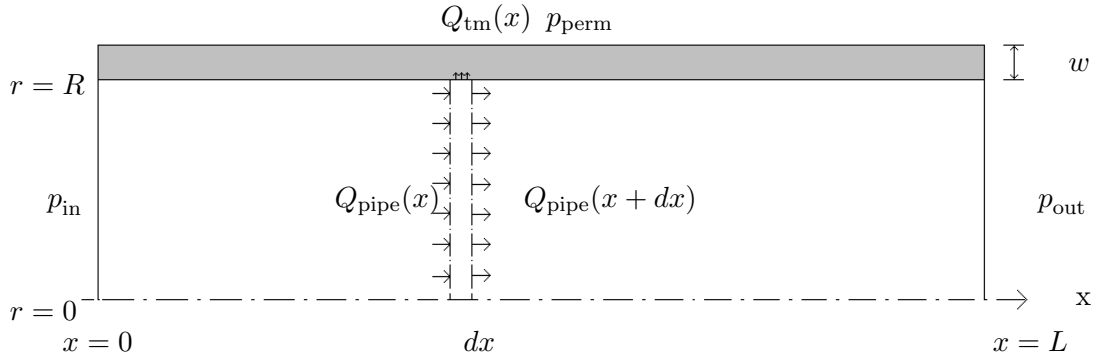
Figure 3.5: *Flow in a porous pipe. The pressures p_{in}, p_{out} and p_{perm} is set constant.*

The boundary conditions are, as see on Fig. 3.5, $p(0) = p_{\text{in}}$, and $p(L) = p_{\text{out}}$. The solution can then be written as:

$$p(x) \quad = \quad \frac{e^{\lambda x}\left(p_{\text{out}} - p_{\text{perm}} - e^{-\lambda L}p_{\text{in}} + e^{-\lambda L}p_{\text{perm}}\right)}{-e^{-\lambda L} + e^{\lambda L}}$$
$$- \frac{e^{-\lambda x}\left(-p_{\text{in}}e^{\lambda L} + p_{\text{out}} - p_{\text{perm}} + p_{\text{perm}}\,e^{\lambda L}\right)}{-e^{-\lambda L} + e^{\lambda L}} + p_{\text{perm}} \qquad (3.21)$$

Using this equation, the pressure difference in the pipe is plotted in Fig. 3.6. The shape of this graph, makes it obvious to try to rewrite Eq. (3.21) using Taylor expansion. The exponential functions become

$$e^{\lambda x} \simeq 1 + \lambda x + \frac{1}{2}(\lambda x)^2, \qquad (3.22)$$

$$e^{-\lambda x} \simeq 1 - \lambda x + \frac{1}{2}(\lambda x)^2. \qquad (3.23)$$

By setting p_{perm} equal to zero, and inserting into Eq. (3.21), it yields:

$$p(x) = p_{\text{in}} + \frac{x}{L}\left[p_{\text{out}} - p_{\text{in}} - (\lambda L)^2\left(\frac{1}{3}p_{\text{in}} + \frac{1}{6}p_{\text{out}}\right)\right] + \frac{1}{2}(\lambda x)^2\left[p_{\text{in}}\left(1 - \frac{1}{3}\frac{x}{L}\right) + \frac{1}{3}p_{\text{out}}\frac{x}{L}\right]$$
$$(3.24)$$
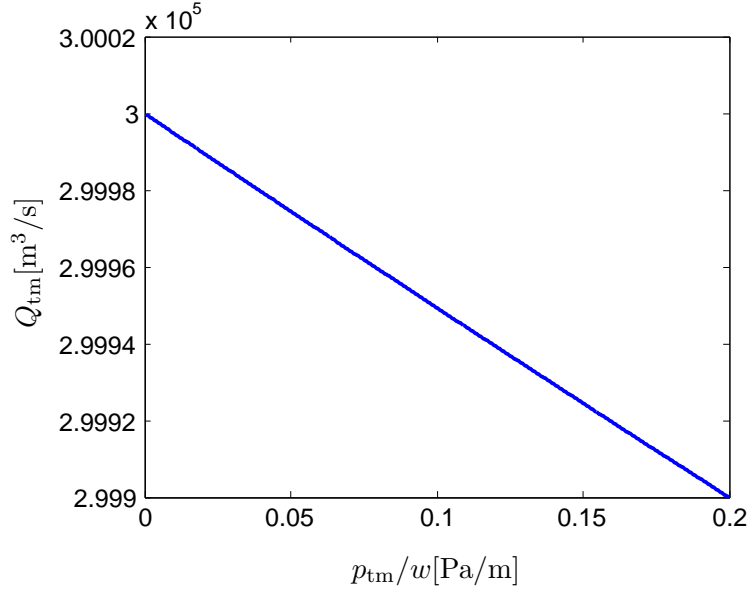
Figure 3.6: *Pressure distribution in a porous pipe with $k = 1.7 \times 10^{-13} m^2$, $\eta = 10^{-3} Pa\,s$. Δp between inlet and outlet are set to 10 Pa. Observe the similarity to a linear function*

As it can be seen from Eq. (3.24), the term $(\lambda\,L)^2$ controls the magnitude of the deviation from a linear pressure drop. By inserting $k = 1.7 \times 10^{-13}$ m^2, $R = 6.5 \times 10^{-3}$ m, $w = 3.5 \times 10^{-3}$ m into Eq. (3.19), and using $L = 0.3$ m following is obtained:

$$(\lambda\,L)^2 = 1.5 \times 10^{-4}. \tag{3.25}$$

As $(\lambda\,x)^2 \le (\lambda\,L)^2 \ll 1$, it can be concluded that if the flow in the pipe is laminar, the pressure drop is linear. To simplify calculations using the pressure difference between the center of the pipe, and the pressure outside the pipe, the trans-membrane-pressure can be approximated by

$$p_{\mathrm{tm}} = \frac{(p_{\mathrm{in}} + p_{\mathrm{out}})}{2} - p_{\mathrm{perm}}. \tag{3.26}$$

According to Ref. [7], the trans membrane pressure in all flow situations in cross flow membranes can be described by Eq. (3.26), which will also be applied in this thesis, on the back ground of the assumptions and calculations made in Section 3.2.1.

3.2.2   General pipe flow

In the previous section, it was assumed that the flow in the pipe was laminar, as the flow was assumed to be a Poiseuille flow. However, this is not the case in most situations, as

the Reynolds number easily exceeds 2000, cf. Ref. [5], which is the limit for laminar flow in a normal pipe flow. Therefore, a friction factor is introduced, which will vary, depending on the characteristics of the flow.

The friction loss in the pipe is caused by the shear stress, which is non-dimensionalized into the friction factor using the dynamic pressure Ref. [5],

$$f = \frac{\tau}{1/2\rho U^2}. \tag{3.27}$$

For a laminar flow, the friction factor is proportional to the Reynolds number in Eq. (2.4) and is defined as

$$f_{lam} = \frac{16}{Re}. \tag{3.28}$$

By inserting the friction factor into Eq. (3.17), the general equation for pressure in a pipe becomes:

$$Q = \frac{r^3 \pi}{\rho U} \frac{1}{f} \frac{\Delta p}{L}. \tag{3.29}$$

In turbulent flow, there is no analytical solution for the friction factor. Yet, well-proved empirical formulae are used. For flow in smooth pipes, the factor is given by

$$f_{turb} = 0.079 \, Re^{-1/4}. \tag{3.30}$$

Inserted into Eq. (3.29), and using Eq. (2.4), it becomes

$$Q = 4.71 \, \pi r^{19/7} \rho^{-3/7} \eta^{-1/7} \left(\Delta p / L\right)^{4/7}, \tag{3.31}$$

which can be rewritten as

$$\Delta p \approx K Q^2, \tag{3.32}$$

where K depends on the characteristics of the pipe and the fluid inside. It is seen from Eq. (3.32) that the pressure drop in a porous tube is dependent on the flow rate squared, compared to that of the laminar flow, where the pressure drop is proportional to the flow rate.

The pressure distribution for the turbulent flow in the pipe is not possible to predict analytically, cf. [23]. It can only be stated that Eq. (3.32) is valid, which is of interest when predicting the influence of the flow velocity in the pipe.

Chapter 4

Experimental setup

The goal of the experiments is to be able to describe the flow in porous SiC-membranes, in order to improve design and functionality. Being the first generation experiments it has been important to simplify the experiments as much as possible. In case this description did not finish, it should at least prepare the ground for future work by others.

The project did not provide neither the time nor the funding to establish an experimental setup from the ground up. Therefore, an existing setup, situated at the Department of Chemical Engineering, was modified to be able to test flow in porous SiC-components. The modified setup is of course not optimal, compared to a setup specially designed for this thesis work, as there are certain limitations specific to the present setup. This had the effect that the porous SiC plugs and pipes had to be produced to fit the setup, and not the other way around. This is important to have in mind when interpreting the results.

4.1   Method

As described in Chapter 3, the velocity, and thereby the mass flux, is only dependent on the pressure difference. Therefore, matching values of pressure and the mass flux were measured in every experiment.

Two fundamentally different test settings were used to investigate the flow in porous SiC, the reason for this being the need to eliminate any irregularities that might occur. The two methods differ in the way the pressure is applied: either a centrifugal pump, or hydrostatic pressure was used in a siphon setting as sketched in Figs. 4.1 and 4.2 .

In the pump setting, the pressure is applied by the pump, which generates a flow in the system. The pressure in the test section can be varied in two ways: By increasing the performance of the pump, or by increasing the resistance of the system. The output of the pump can be controlled continuously, and the resistance of the system is controlled by a screw valve, which also can be varied continuously.
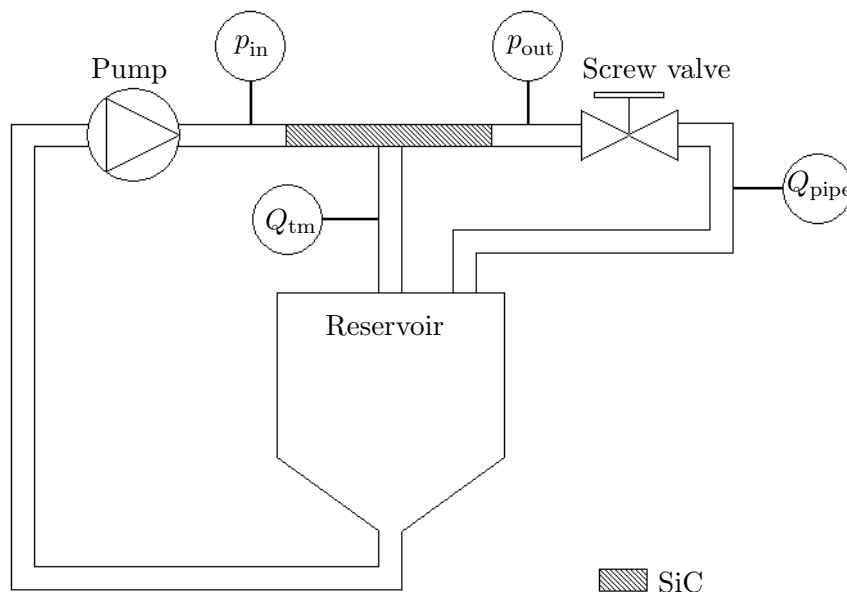
Figure 4.1: *Sketch of the pump-driven test setting. The pressures p_{in} and p_{out} were measured by electric manometers connected to a computer. The flow rate Q_{tm} through the membrane was calculated from the mass flow measured by a weight, and the pipe flow rate Q_{pipe} was measured by a flow meter. The trans membrane pressure was calculated from the inlet and the outlet pressures.*

4.1.1   Test equipment

Working fluid

The working fluid in all experiments was demineralized water. This was chosen partly because of the easy access in the laboratory, partly because water, or an aqueous solution is by far the most used working fluid in filtration.

Pump

The pump was a centrifugal pump with variable adjustment of output, with a maximum power of 0.37 kW.

Pipes and hoses

The hoses used are all rubber hoses, with a diameter of 10 mm. In the first two series of experiments, the SiC-component for testing was mounted in a circular stainless steel housing, with two exits for permeate, see Fig. 4.3.

Depending on the experiment, either no, or just one exit was utilized. On each side of the steel housing, a steel connection to the hose was mounted, each with a manometer, see Fig. 4.4.
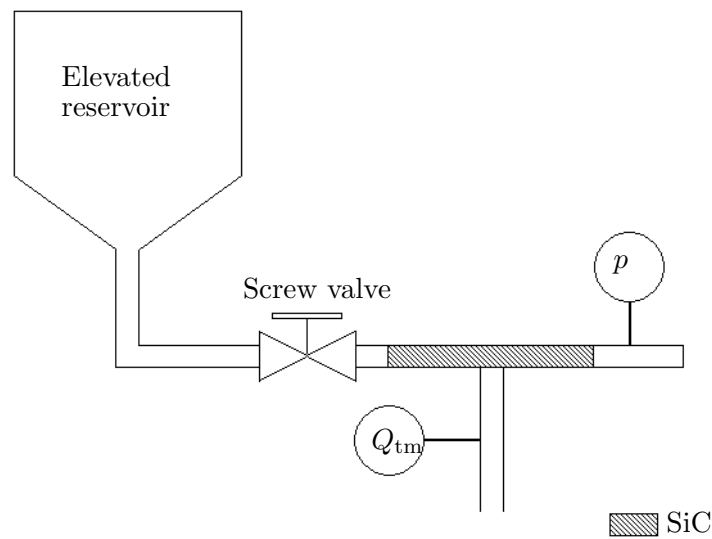
Figure 4.2: *The functional sketch of the siphon setting. The pressure is applied in the left hand side of the setting. The pressure is calculated from a measured height difference between the reservoir and the porous pipe. The manometer was mounted for calibration purposes*

Sealing

All o-rings are made of rubber. Besides o-rings, insulation tape and teflon®tape has been used for sealing purposes in the junction of the different parts.

Data acquisition and data processing

Data has been collected on a computer: HP, Pentium 75, 66 MHz. 16 Mb RAM, using the program: "Eclipse", ®1993, Per Stubbe. The program collected the measured data at a rate of 4 Hz.

Each measurement was collected into a file, which was processed in MatLab, see the

Figure 4.3: *The steel housing, in which the SiC-components were mounted. Either none, or just one permeate exit was used in each experiment.*

script in Section A.2. The pressure measurements were filtered for spikes occurring at low pressures, and the flow rate was calculated from the mass flux.

Pressure measurement

The pressure was measured at the inlet and at the outlet of the steel housing using electric Haenni manometers, which could be connected to a computer. They were able to measure pressure from 0 to 6 bars. To assist with the adjustments of the pressure, analogue manometers were also mounted, see Fig. 4.4.
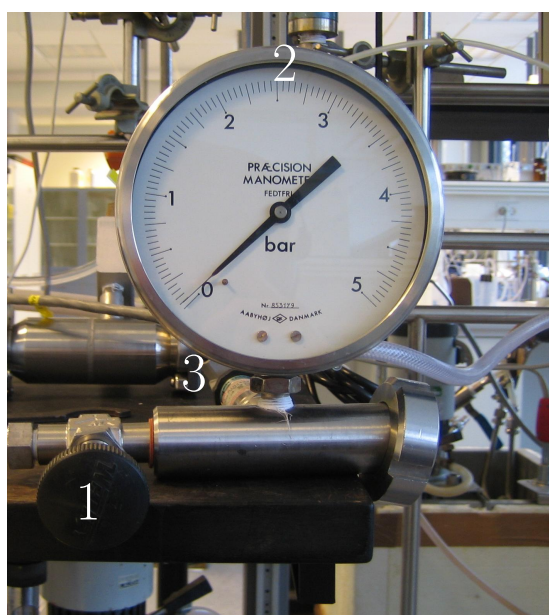
Figure 4.4: *The type of manometers used in the experiments. 1: Screw valve, used to control the flow rate in the pipe. 2: The analogue manometer, for easy estimation of the pressure level. 3: The digital manometers were mounted on the back of the analogue manometer. The pressures used in the data processing was solely measured by the digital manometers.*

The pressures were measured as gage-pressures, i.e. pressures compared with the atmospheric pressure. It was assumed that the permeate pressure, p_{perm}, had a gage pressure equal to zero. A typical measurement of the pressure can be seen in Fig. 4.5.

As the system needed to stabilize to get a constant pressure measurement, not all measured data was used. The initial data were discarded, such that only data from a steady system were used to calculate the pressure gradient. The data range used can be seen in Fig. 4.5. The standard deviation of the pressure measurements varied from 1500 Pa to 3500 Pa. Every pressure measurement was averaged over a certain time period. It was assumed that the variations observed in the pressure was due to the operational principle of the pump.
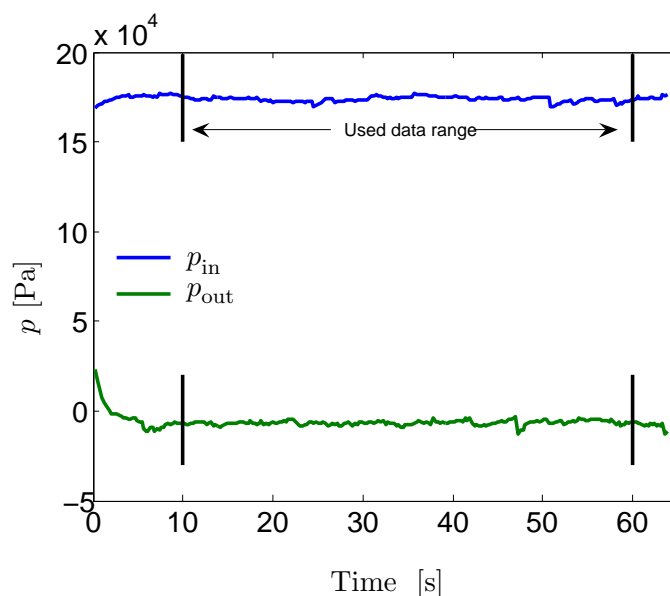
Figure 4.5: *Raw data from a typical pressure measurement.*

It was observed during the experiments that the manometers had a slight deviation from zero gage pressure when no pressure was applied. Therefore, prior to each measurement, this offset was measured, and subtracted from the measured pressure.

Flow rate measurement

The flow through the porous pipe was measured by continuously logging the digital weight on the computer. The weight, of the brand "Mettler Toledo", was able to measure mass with an increment of 0.01 g $= 10^{-5}$ kg. The flow rate was then simply calculated by

$$Q = \frac{1}{\rho} \frac{\mathrm{d}M}{\mathrm{d}t}. \tag{4.1}$$

with $\mathrm{d}M$ being the mass increment, $\mathrm{d}t$ the time increment, and the density for water at 20 °C, $\rho = 998$ kg/m^3.

The flow through the pipe, Q_{pipe}, was measured by a flow meter, with a scaling from $F = 0 \ldots 100$. This scale was converted into volume flux using the calibration equation

$$Q_{\mathrm{pipe}} = 2.4050 \times 10^{-6} F + 1.2063 \times 10^{-5}. \tag{4.2}$$

given by Ref. [22]. This flow meter was the only measuring device in the setup, which was not directly connected to the data acquisition program on the computer. Each value is visually observed, and the Q_{pipe} was calculated using Eq. (4.2).

Siphon-setting

The siphon was made of a rubber hose, with a diameter of 25.4 mm. The valves mounted was standard shut-off valves for Ø25.4 mm hose. The branches of the setting was made by copper t-pieces.

The reservoir had a diameter of 350 mm, and a volume of $\mathcal{V}_{res} = 25$ L.

4.1.2   SiC

The properties of the experimental equipment at hand made it advantageous to consider two geometries of the SiC: A circular plug and a pipe, see Fig. 4.6. The dimensions of these were determined by the existing extruder at CoMeTas A/S, and it was not possible to change these geometries.
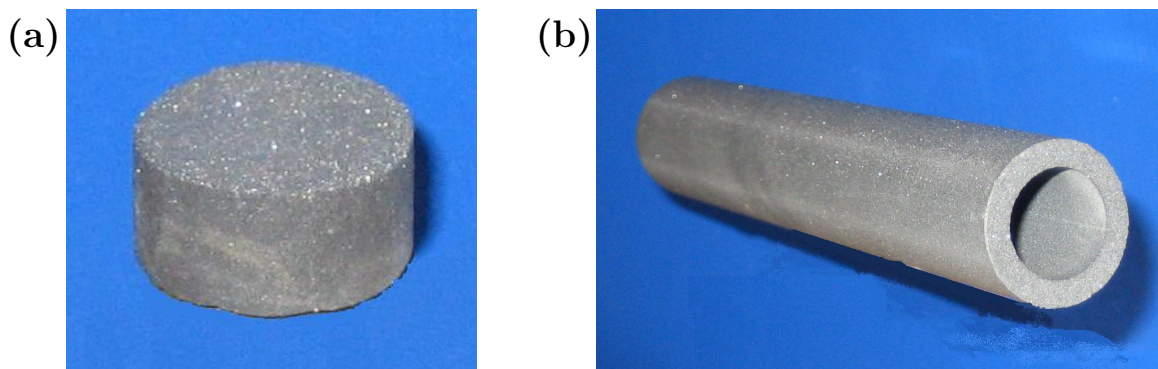
Figure 4.6: *(a) Porous plug with radius $R = 11.7$ mm and length $w = 12.5$ mm. The plug was made of F220 clay, yielding pore sizes from 12 μm to 15 μm. (b) Porous pipe, with inner radius $R = 10$ mm, wall thickness $w = 3.5$ mm, length $L = 165$ mm. The porous pipe has a pore size around 10 μm, which was estimated from SEM-pictures, as the type of clay was unknown..*

Both geometries were made from extruding a clay of SiC particles, and then burning them at 2300 °C. The plugs are made from a solid cylinder of SiC, which has been extruded, dried and burned and then cut into the desired lengths. To produce the porous pipes, an insertion to the extruder was made, see Appendix (A.1). With this mounted, the extruder would extrude a pipe in the desired dimensions, instead of a solid cylinder.

4.2   Conduct of experiments

The pressure was adjusted manually on the setup, and a new file was created on the computer for each measurement.

4.2.1 Plug flow

The characteristics of the flow were investigated by alternating the pressure, and the length w of the plug. A total of five different lengths were used in the plug flow experiments, see Fig. 4.7. Moreover, two types of SiC-clay yielding two different pore sizes was employed. It was not possible to determine the exact mean pore size of the plugs, as it varies in a interval, taken from Ref. [11]. Plug 3 had a pore size of $6 - 10$ μm and plug 6 had a pore size of $12 - 15$ μm Ref. [11]. These two plugs were used in the experiments, and then cut into shorter plugs. The procedure of cutting the short plugs from the long made it possible to investigate the length dependence. Plugs 1,2 and 5 are not shown in Fig. 4.7 as they were discarded due to fractures.

$w = 11.0$ mm $w = 7.0$ mm $w = 22.5$ mm $w = 12.5$ mm $w = 8.0$ mm
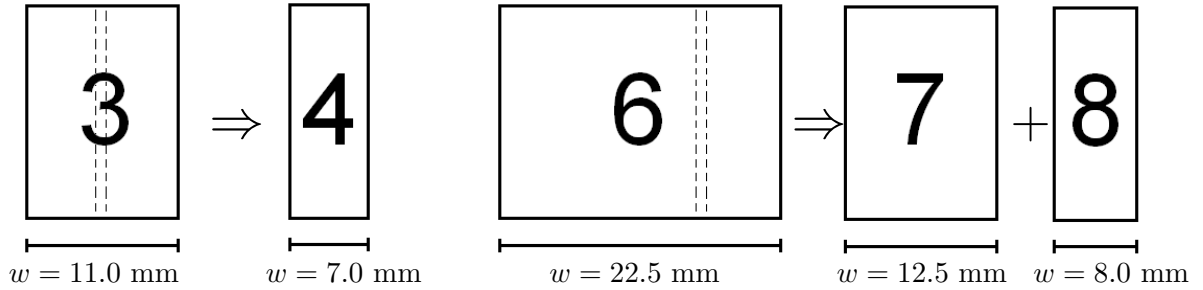
Figure 4.7: *Different plugs used. Plug 4 is cut from plug 3, and have mean pore size of 6 $\mu m - 10$ μm. Plugs 7 and 8 are cut from plug 6, and have a mean pore size of 12 $\mu m - 15$ μm.*

To avoid any leaks from the plug, besides the flow through the porous material, the sides of the plug was sealed by teflon tape, and fastened in the pipe with an o-ring of rubber. The plug was prevented from slipping on the o-ring by a stainless steel ring, with a diameter slightly smaller than the plug, see Fig. 4.8. The plug was mounted by pressing the plug and the o-ring into the steel housing, using an iron pipe.
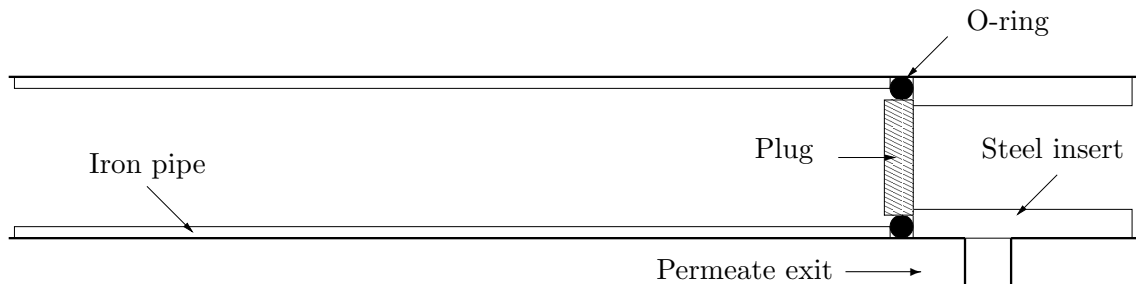
Figure 4.8: *Mounting of the plug in the steel housing. The flow comes from left to right. The diameter of the steel insert is slightly smaller than the diameter of the plug in order to hold the plug. The permeate exit was blocked by the steel insert, and not in use.*

The mass flow was calculated by continuously weighing the liquid penetrating the plug. The logging time was 0.25 s, 4 measurements per second. This frequency was assumed to be sufficient, as the flow at low pressure differences was droplets with a lower dripping frequency of approximately 1 Hz.

For each plug, 5 different pressures were measured, from about 0.6 - 0.8×10^5 Pa to 3.8 - 4.0 × 10^5 Pa with an increment of 0.8 × 10^5 Pa. When the pressure had settled the mass flow was logged in 60 s, and then averaged.

Each time a new plug was inserted, the pump was set to run around 10 min, to ensure that all air bubbles had been eliminated from the pipe. When the experiments ended, the plug was investigated for any change during the test period, for example particles in the flow etc.

4.2.2 Pipe flow

The porous pipe used in this experiment was 0.165 m long, and had an estimated pore size around 10 μm and an estimated porosity of 45%. These parameters were estimated from Fig. 4.9, which is a SEM-picture of a random cross-section in the pipe.
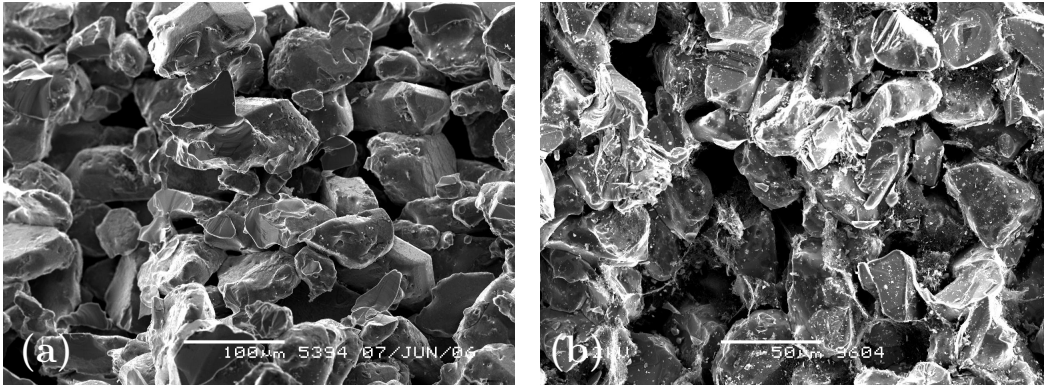
Figure 4.9: *SEM-pictures of the porous pipe. (a) A picture of a solid matrix with a pore size range of* 15 μm $-$ 25 μm, *notice the white* 100 μm *bar (b) The bulk of the porous pipe. By comparing the white* 50 μm *bar with the the white bar on (a), it is roughly estimated, that the particles are approximately half the size of (a), yielding a pore size of* 10 μm. *Also from the white* 50 μm *bar, the largest particle sizes are seen to be of the order of* 35 μm, *not to be confused with the mean particle size, which is assumed to be* 35 μm. *Observe the large number of scattered small particles, which appears as white dots.*

The flow rate in the pipe, Q_{pipe}, was varied linearly from 2.4×10^{-5} m^3 to 14.0×10^{-5} m^3, which was the maximum performance of the pump, with an increment of 0.7 × 10^{-5} m^3. For each flow rate, the inlet pressure p_{in}, and the outlet pressure p_{out} were logged, and the pressure drop calculated.

Normal setting

The system for investigating the flow in porous pipes is the same as for the plug-flow. The setting differs only in the mounting of a porous pipe in the steel housing, as seen in Fig. 4.10.
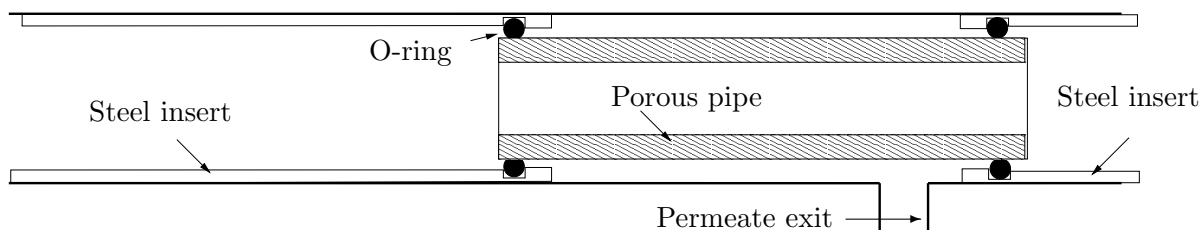
Figure 4.10: *The porous pipe in the steel housing is mounted using o-rings. Metal inserts are designed to fix the o-rings, in order to prevent leaks.*

In contrast to the plug flow, the exit on the side of the steel housing was used to measure the flow through the porous walls for the open pipe experiments.

In order to increase the accuracy of the experiments, the setting was altered in the blocked pipe experiments, to be able to measure pressure and flow rates without the steel housing. Using this configuration, the assumption that $p_{\mathrm{perm}} = 0$, was bound to be valid. It also became possible to visually inspect the sealings for any potential leaks. The free-air mounting of the porous pipe was also used in the siphon setting.

Siphon setting

As described in Section 4.1.1, the pump creates fluctuations in the pressure, making it impossible to get usable measurements at low pressures. Due to this, the setting using the principle of a siphon was developed. The advantage of using this method to apply pressure, was the simplicity. The pressure applied equals the hydrostatic pressure of height h which is the distance between the water surface inside the container in the top, and the shut-off valve

$$\Delta p = \rho g h, \tag{4.3}$$

where h is easy to measure.

Simply put, a siphon is a continuous tube that allows liquid to drain from a reservoir through an intermediate point that is higher than the surface level of the reservoir, as seen in Fig. 4.11. The flow is driven only by the hydrostatic pressure of the water column. It is necessary that the final end of the tube be lower than the liquid surface in the reservoir.

In the siphon created for the present experiment, there is not necessarily a flow. After initiating the flow, the end of the pipe is shut off by a valve. The static pressure on the valve will then be the hydrostatic pressure, exerted by the water.
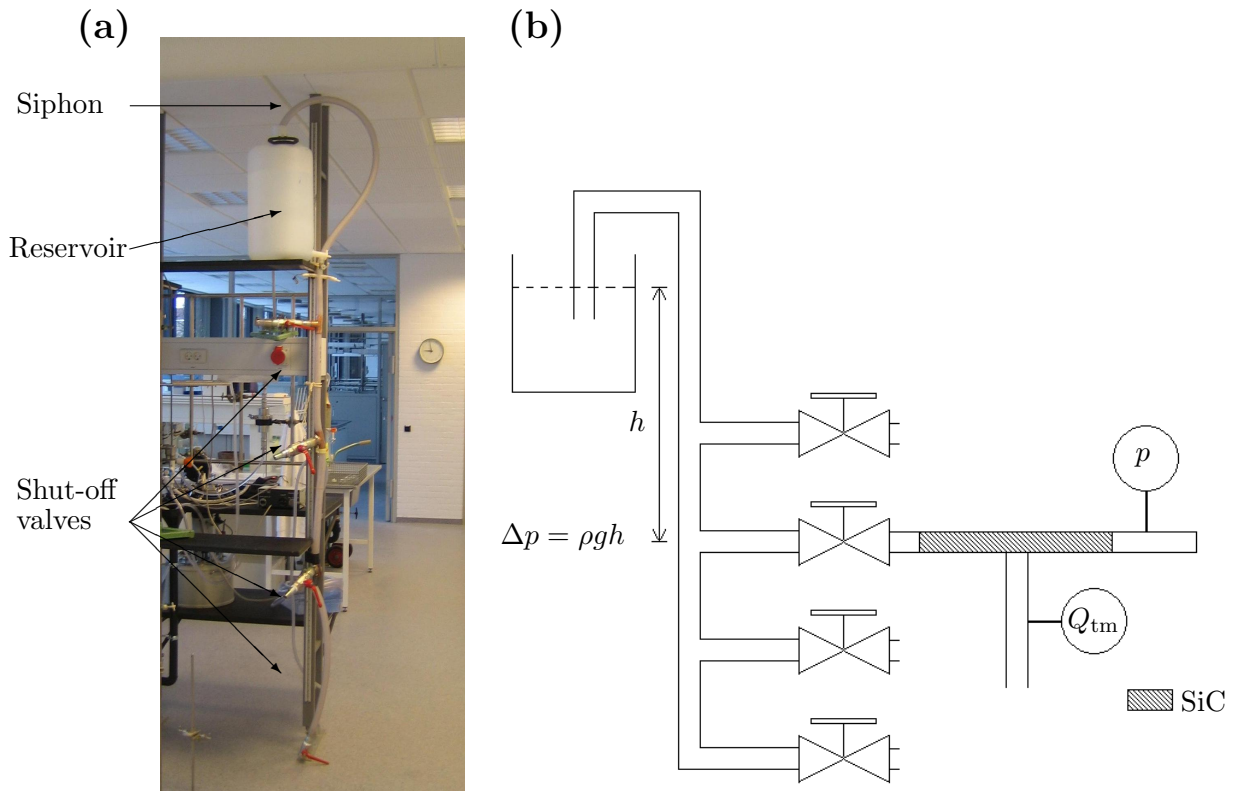
Figure 4.11: *(a) The siphon setting as it appeared in the laboratory. (b) The principle of the siphon. The porous pipe could be moved to each shut-off valve, which thereby changed the pressure.*

The four exits, combined with changing the height of the water surface in the reservoir, made it possible to obtain pressures from 0.5×10^4 Pa to 2.0×10^4 Pa with an increment of 0.25×10^4 Pa.

4.3 Potential uncertainties in the test setting

During the conduct of experiments, it is unavoidable to experience variations of the results, which can lead to misleading, or in the worst case scenario, false conclusions, if not properly taken into account. In this section, it is attempted to consider any uncertainty that might affect the outcome of the experiments.

4.3.1 Production of the porous SiC-components

As described in Chapter 2, the SiC-components are made of a clay, which, when heated, produces porous SiC. The process of making the plugs consisted of several steps: extrusion, drying, burning and cutting. Every step can be the source of anisotropy in the medium.

When the clay is extruded, the amount of stress applied has to be high enough to compress the clay to create a uniform cylinder. If this fails, there will be small pockets of air trapped in the plug or pipe, which will lead to cracks.

The process of drying the SiC-component may also affect the properties, because if dried too fast, cracks can form.

Burning porous SiC can lead to anisotropy if not controlled properly. As the plugs were specially made to this project, there were no experience of which temperature the burning should reach. Again, if the temperature was to high or too low, cracks could be created.

To be able to change lengths of the plugs, the solid cylinder were cut into smaller pieces. If excess particles from this process failed to be removed, the would block the pores, yielding a lower permeability at the ends.

4.3.2 Pore sizes of the porous SiC

The information available concerning the pore sizes of porous SiC was not specific, i.e. the pore sizes was given in a range varying up to 30%. The best estimation of the mean particle size was to assume the same size as the pore size, justified by a porosity close to 50%.

With all these assumptions taken into account, it was estimated that the permeability could vary up to 40% for the clays used.

4.3.3 Flow rate measurement

Leaks and sealing and cracks in the porous media

If the sealing of the SiC-component fails, an increase in measured permeate flow rate will be measured. Extreme care is therefore important when mounting the porous plug or pipe, as a small leak can have a great effect on the outcome of the experiments.

A simple sensitivity analysis has been made to investigate the influence of potential cracks in the porous components. The flow rate, Q_c, in an ideal circular straight crack with radius r in a plug with the length w, can be calculated by laminar flow theory

$$Q_c = \frac{\pi}{8} \frac{r^4}{\eta w} p_{\mathrm{tm}} \tag{4.4}$$

with p_{tm} as the pressure difference. Assuming that this is the only crack, and that the flow rate Q_{tm} in the porous component, in this case a plug with radius R, and a permeability of k without the crack, is governed by Eq. (2.18), the relative change C in the flow rate through the plug is

$$C = \frac{Q_c + Q_{\mathrm{tm}}}{Q_{\mathrm{tm}}} \tag{4.5}$$

which yields

$$C = 1 + \frac{r^4}{8kR^2} \tag{4.6}$$

when inserting. This result indicates, that if a porous SiC plug has a permeability of $k = 3.0 \times 10^{-13}$ m^2 and a radius of 11mm, a crack, or a leak of the sealing with a diameter of 0.1mm, will result in a total permeability of $k = 4.0 \times 10^{-13}$ m^2, i.e. an increase of 33%. It can therefore be concluded, that even the slightest crack, can have significance in the calculation of permeability.

Evaporation

As the volume flow was calculated by continuous logging of the weight of the water penetrating the plug, evaporation from the weight has to be considered. By measuring 10 minutes, a total of 1.1×10^{-3} kg of water evaporated, yielding a flow rate of

$$Q_{evap} = 1.9 \times 10^{-9} \text{ m}^3/\text{s}. \tag{4.7}$$

As the volume flow from the main flow is expected to be in the order of magnitude of 10^{-6} m^3/s, evaporation is neglected.

It was observed that the water temperature rose to 26°C during a day of experiments, due to the work performed by the pump on the water. However, as the density for water at 26°C temperature is $\rho = 997$ kg/m^3 [1], this slight change was not considered. However, the viscosity changes from $\eta = 10^-3$ to $\eta = 0.9 \times 10^-3$ during the same temperature rise. This has to be taken into account, when processing the data from the experiments.

It was assumed that if erroneous results occurred, it would not be due to effects from the surrounding environment, e.g. draft and temperature changes in the laboratory were neglected.

4.3.4 Pressure measurements

Manometers

The manometers in the setting is connected to a computer, which made it possible to examine their characteristics. During the experiments, it was necessary to calibrate these manometers by measuring the pressure when no pressure was applied.

Loss

During pre-tests of the setting, a leak was located at a joint of the feed hose from the pump, and was placed immediately before the manometer placed at the inlet, see Fig. 4.1. It was concluded that this leak was insignificant, as the pressure difference over the plug is the main parameter. The leak did not have any effect on the flow through the plug as a function of the pressure difference.

---

[1] Density values calculated from Ref. [3]

4.3.5 Human factors

When conducting experiments, there is always a possibility of human mistakes. These are attempted to be minimized by being aware of the factors described in this section.

The measuring time for each experiment has been found on the basis of the experiments, i.e. when the system was stabilized, measurements were initiated. From the staff at the laboratory it was advised that 30 s was the normal measuring time on the setting. To be sure, the measuring time for the present experiments were 60 s for the majority of measurements.

Chapter 5

Plug measurements

The results of the plug experiments are presented and discussed in this chapter. These are used as an indication of the basic flow in SiC, which will be used in the preceding experiments.

5.1 Expected results

As described in previous chapters, it was expected that the flow in the plugs would obey Darcy's law. If a linear relationship is established, it will be possible to calculate the permeability of the plug by rearranging Darcy's law to

$$k = \frac{\eta w}{\pi R^2} \frac{Q}{\Delta p},$$

(5.1)

with w being the length of the plug, and R being the radius. By conducting a simple measurement of the geometry and the weight, of the sample, it was possible to make an estimate of the porosity, by stating following equation:

$$\phi_{plug} = 1 - \frac{\mathcal{V}_{\mathrm{SiC}}}{\mathcal{V}_{\mathrm{tot}}},$$

(5.2)

where $\mathcal{V}_{tot} = R^2 \pi w$ and $V_{\mathrm{SiC}} = M_{\mathrm{plug}}/\rho_{\mathrm{SiC}}$. For all the plugs, the porosity was calculated to

$$\phi = 46\%,$$

(5.3)

which is consistent with the value of the porosity of porous SiC of 45% stated by Ref. [8].

As the type of clay is known for the production of the plugs, it is possible to place the mean particle size in the range of

$$d_m = 6 \ \mu\mathrm{m} - 10 \ \mu\mathrm{m},$$

(5.4)

for plug 3 and 4, and

$$d_m = 12 \ \mu\mathrm{m} - 15 \ \mu\mathrm{m}$$

(5.5)

for plug 6, 7 and 8 as described in Section 4.3.2

Using the Kozeny-Carman equation, Eq. (2.17), the permeability is assumed to be in the range of

$$k_{\text{expected}} = 0.6 \times 10^{-13} \text{ m}^2 - 1.7 \times 10^{-13} \text{ m}^2 \tag{5.6}$$

for plug 3 and 4, and

$$k_{\text{expected}} = 2.4 \times 10^{-13} \text{ m}^2 - 3.8 \times 10^{-13} \text{ m}^2. \tag{5.7}$$

Ref. [11] states a permeability of SiC in the area of

$$k_{\text{table}} = 3.0 \times 10^{-13} \text{ m}^2. \tag{5.8}$$

for plug 3 and 4, and

$$k_{\text{table}} = 5.0 \times 10^{-13} \text{ m}^2. \tag{5.9}$$

for plug 6, 7 and 8. These ranges of permeabilities are calculated assuming spherical particles, in order for Eq. (2.17) to be valid. The SEM-pictures in Fig. 4.9, Section 4.2.2, show, that the particles in porous SiC are not spherical. The expected results are stated here to give an impression of the order of magnitude of the permeabilities.

5.2   Results

Assuming validity of Darcy's law, Eq. (2.18), the measured quantities should produce a straight line in a plot of the flow rate and the pressure gradient. By knowing the viscosity of the fluid, it is thereby possible to calculate the permeability from the inclination by of the fit of each graph by using Eq. (5.1).

5.2.1   Plug 3 and plug 4

Plug 3, and thereby plug 4, is made from F240 clay, which produces porous SiC with pore sizes from $6-10$ μm, Ref. [11]. Fig. 5.1 shows the results from these two plugs. Both series show linearity, as expected. However, it was also assumed that the permeability should be constant, i.e. independent of the length of the plug. The difference in the permeability k is calculated to 21 %. The main explanation for this difference is assumed to be irregularities in the porous medium, e.g., cracks or dust from cutting as described in Section 4.3.

The Reynolds number based on grain diameter is calculated to

$$\text{Re} = 0.2, \tag{5.10}$$

which, according to Chapter 2, makes it reasonable to assume flow in the Darcy region.

The most plausible explanation of the deviation is assumed to be an anisotropic solid matrix structure of plug 3, caused either by cracks formed during production, or by excess particles from the act of cutting the plugs. If smaller particles has failed to be removed, they could block the pores in the plug, and thereby decrease the permeability. This would fit the results, as the permeability is decreased subsequent to the cutting.
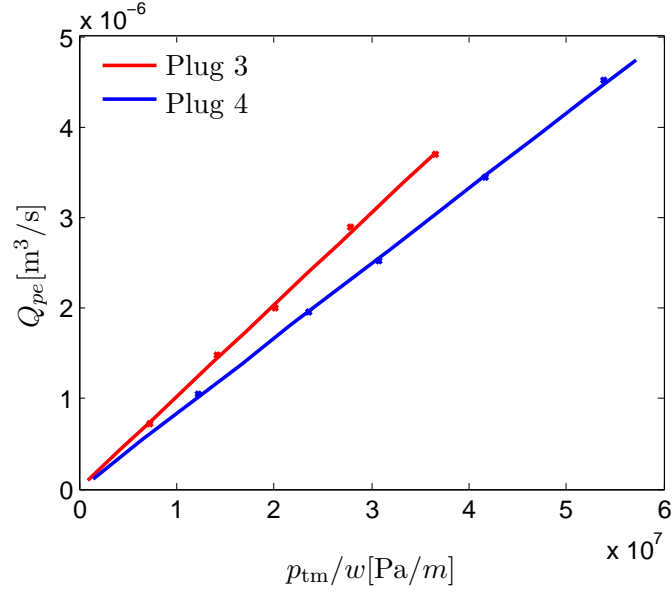
Figure 5.1: *Fit of plug 3 and plug 4, $k_{p3} = 2.4 \times 10^{-13}$ m^2, $k_{p4} = 2.0 \times 10^{-13}$ m^2. The permeabilities should be identical, as plug 4 is cut from plug 3.*

5.2.2   Plug 6, plug 7 and plug 8

Plug 6, and thereby plug 7 and 8 was made of F220, which produces porous SiC with pore sizes $12 - 15$ μm. Plug 6 was, after the first measurements, cut into two halves, plug 7 and 8.

Fig. 5.2 shows the results from plug 6, plug 7 and plug 8. Again, a decrease in the permeability was observed, as the plugs decreased in length. Plug 7 has a permeability of 94% of plug 6, whereas plug 8 has decreased to 64%.

The fact that both permeabilities has decreased makes it plausible that several effects has to be considered. If the decrease was solely due to anisotropy, one would expect one permeability higher than the original, to compensate for the decrease. Effects from the cutting seems reasonable to consider, as they would decrease the permeabilities in both plugs. However, it must be assumed that plug 7 and plug 8 should have the same relative reduction in permeability, which is not the case.

5.2.3   Hysteresis

A part of validation for the set-up was to investigate the significance of the pressure being adjusted from a higher pressure to a lower pressure or vice versa. Fig. 5.3 shows a series
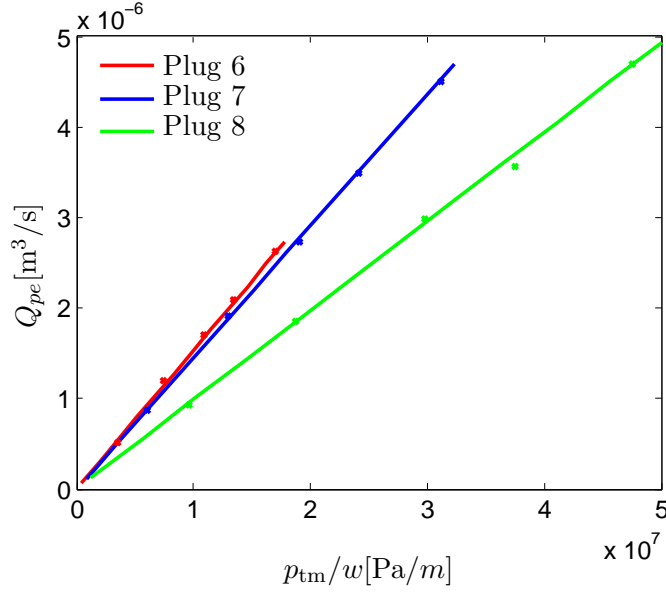
Figure 5.2: *Fit of plug 6, plug 7 and plug 8,* $k_{p6} = 3.6 \times 10^{-13}$ *m*^{2}, $k_{p7} = 3.4 \times 10^{-13}$ *m*^{2}, $k_{p8} = 2.3 \times 10^{-13}$ *m*^{2}. *Plug 7 and plug 8 are cut from plug 6.*

of measurements, where the pressure was adjusted from 0 to 4 bar, and back to 0. It is obvious that the inclination of the curves are equal, but there is some hysteresis.

5.3   Conclusion of the plug experiments

It was verified that the relationship between the flow rate and the pressure gradient was linear for all plugs. From the slopes of the linear curves the permeability of the plugs was calculated to a value in the same range as expected, as all permeabilities were between $k = 2 \times 10^{-13}$ m^2 and $k = 4 \times 10^{-13}$ m^2. The largest deviation from the expected permeabilities was calculated for plug 3 and 4. It is argued, that this was due to cracks in the plug.

It was observed that the permeability dropped for the short plugs, compared to the long. This was not expected, as a prerequisite for validity of Darcy's law is constant permeability. This deviation is explained by effects occurring at the entrance to the plug, e.g. dust from the cutting.

In one of the experiments, it was possible to show validity of Darcy's law within 10%, where other showed deviations up to 38%.

It is concluded on the basis of the results, that Darcy's law is indeed applicable in
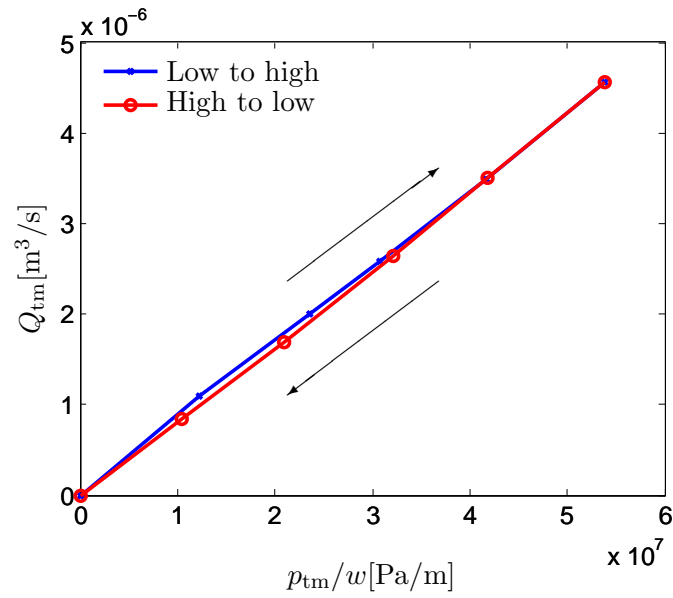
Figure 5.3: *Graph for plug 4. The pressure is adjusted from low pressure to high pressure, and then back to low. Notice the linearity, which indicates the validity of Darcy's law*

porous SiC. However, large deviations can occur due to uncertainties.

The main result of the plug experiments was that Darcy's law was applicable, i.e. a linear relationship could be established, and the measured k agreed with the predicted.

Chapter 6

Open pipe experiments

The open pipe experiments are conducted with a primary flow, Q_pipe through the pipe, and with a secondary flow Q_tm through the porous wall. The subscript tm stands for trans membrane.

In the open pipe experiments, the initial measurements were conducted in order to determine the hydraulic resistance of the flow between the two manometers.

The subsequent experiments were focused on the effect of the primary flow in the flow rate through the pipe, and on the validity of Darcy's law.

In analogue with Section 5.1, the porosity of the pipe was calculated to

$$\phi = 45\%. \tag{6.1}$$

The type of clay used for making the porous pipe was not known. Therefore, the particle size of the pipe was estimated by comparing a SEM-picture of the porous pipe with a picture of porous SiC with known mean particle size, see Fig. 4.9 inSection 4.2.2.

The particle size is estimated to

$$d_m = 10 \ \mu\text{m} \tag{6.2}$$

and the expected permeability to

$$k_\text{expected} = 1.67 \times 10^{-13} \ \text{m}^2 \tag{6.3}$$

using Eq. (2.17).

These estimated values are associated with great uncertainties as described in Section 4.3, and are only used as an indication.

6.1 Pressure drop in pipe

In Section 3.2.2 it was assumed that the flow in the pipe was turbulent. In the open pipe experiments, the this was investigated by removing the porous pipe from the steel housing, and then measuring the flow rate from the permeate exit. The flow through
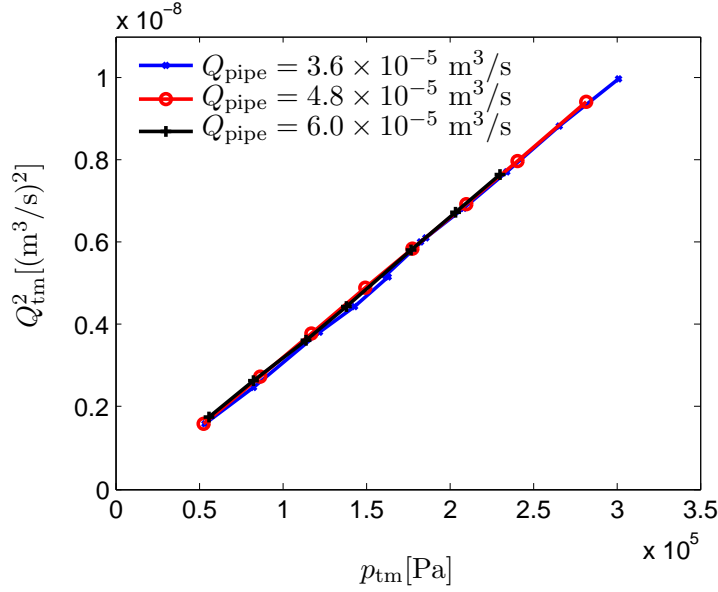
Figure 6.1: *The square of the flow rate from the permeate exit as a function of the pressure in the steel housing. The fact that the data yields straight lines verifies the turbulent flow in the system, without a porous pipe inserted.*

the steel housing was kept constant, and the experiment was repeated for three different values.

It can be concluded from Fig. 6.1 that the flow in the experimental setup without the porous pipe was turbulent. The generation of turbulence mainly originates in the pump and at the inlet and outlet of the system, as the flow rate through the steel housing did not affect the shape and magnitude of the graph in Fig. 6.1.

The pressure drop between the inlet and the outlet of the porous pipe was calculated, and plotted in Fig. 6.2. It is seen that the measured pressure drop in the pipe is not increased, all though the flow velocity is over five times as large. This should be compared with Eq. (3.32), which states that the pressure drop is dependent of the flow rate squared. It can therefore be concluded that pressure drop in the pipe is not significant in the present investigation.

6.2   Flow through wall

This experiment was conducted with a constant flow rate in the pipe, Q_{pipe}, using the same setting as in the previous section with an open exit for permeate. The trans membrane
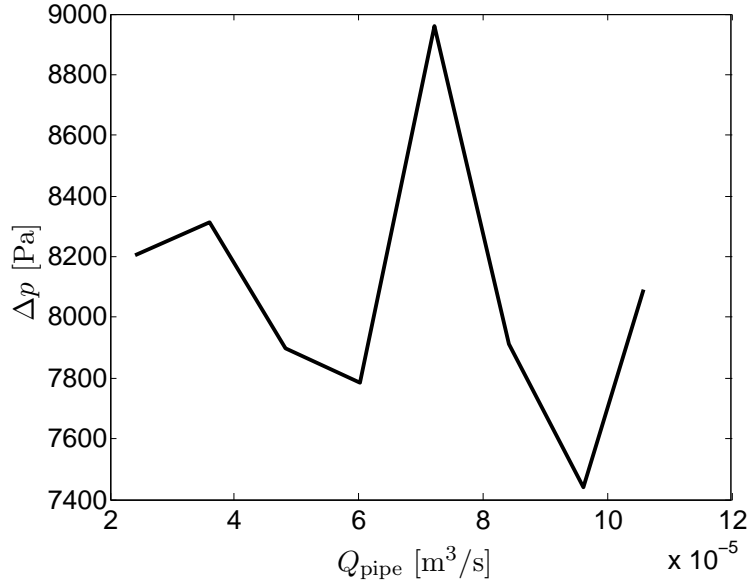
Figure 6.2: *The pressure drop, Δp between the two manometers in the test setting. The relatively large fluctuations of the pressure drop measured in the setting can be related to the fluctuations of the pressure, as mentioned in Section 4.1.1.*

pressure p_{tm} was varied from 0.2×10^5 Pa to 10^5 Pa, and was repeated three times, for values of $Q_{pipe} = 3.6 \times 10^{-5}$ m^3/s, 4.8×10^{-5} m^3/s and 6.0×10^{-5} m^3/s.

Fig. 6.3 shows that velocity of the primary flow in the pipe does no affect the flow through the porous walls, as the graphs for Q_{pipe} coincide.

It was expected that the permeate flow would obey Darcy's law, as indicated in previous chapters. However, the graphs on Fig. 6.3 is not linear.

There are several cases, in which flows in porous media are not linear: it can be characterized as a pre-Darcy flow, or it will be influenced by turbulence, making it a Forchheimer flow, or fully turbulent depending on Reynolds number. Turbulence extracts energy from the flow according to Section 2.1, hence the resistance measured in the porous media will increase. It the present situation, the resistance measured decreases with increasing pressure gradient, which could imply pre-Darcy flow. Throughout the thesis, any non-linear flow, which is above proportional is denoted as a pre-Darcy flow. The demarcation parameter for distinguishing between the different flow parameters is the Reynolds number in Eq. (2.4) using the particle diameter as length scale, and is calculated to
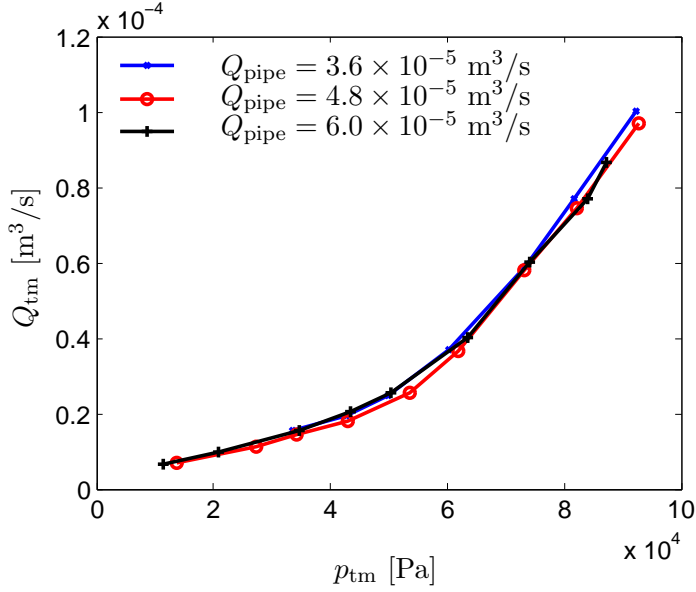
Figure 6.3: *Flow rate through pipe, Q_{tm}, for different flow rate in pipe Q_{pipe}. The experiments were conducted during two days, which confirms the ability to reproduce results. Observe that the relation is above proportional, indicating pre-Darcy flow.*

$$\text{Re} = \frac{\rho Q d_m}{D \pi L \eta} = 10^{-2}, \tag{6.4}$$

for the lowest flow rate. This is several orders of magnitude larger than the limit given as Re $= 10^{-5}$. The explanation for this deviation from previous experiments with other porous materials could be purely material specific, it could be errors occurring during the experiment, or a mix of these possibilities.

6.3   Conclusion of the open pipe experiments

From this series of experiments it can be concluded that the pressure drop in the pipe is insignificant to the results, as it showed not to be possible to establish an increasing pressure drop for increasing flow as the theory predicted.

It was also found that the primary flow in the pipe does not affect the permeate flow in this case, as the same relationship between flow rate and pressure gradient was found at varying flow rates in the pipe. It was already assumed that the pressure drop in the pipe would be insignificant, and this experiment concludes that no other effects, originating in

the primary flow, are significant for the permeate flow.

The absent linearity of the flow rate as a function of the trans membrane pressure was not expected. It was therefore decided to make a further investigation to validate these results, or to confirm applicability of Darcy's law. It was therefore obvious to alter the test setting, which leads to the blocked pipe experiments in the following chapter.

Chapter 7

Blocked pipe experiments

The plug experiments showed validity of Darcy's law, which failed in the open pipe experiments. It was therefore attempted to make the pipe setting similar to the plug experiments by completely shutting the screw valve at the end of the pipe. The pipe would therefore become a plug, the only difference being the geometry. The pipe used in the experimental setup was the same as in the open pipe experiments.

The blocked pipe experiments become a natural extension to the open pipe experiments, as any irregularities relating to the flow through the pipe will be eliminated. The goal is to obtain as accurate results as possible, to confirm or invalidate the indication of a pre-Darcy flow, showed by the open pipe experiments.

7.1 Test setting modifications

To anticipate potential problems with the sealing, the steel housing was removed. This had the effect that the pipe was in free air, such that potential leaks immediately could be visually detected. In addition to this, the area, from where the fluid was collected, was decreased as seen in Fig. 7.1. With this reduction of the length, it was possible to completely rule out potential leaks of the o-ring holding the pipe.

The porous pipe was cleaned in a 0.2% solution of NaOH[1] to attempt to prevent potential foreign matter from blocking the pores.

7.1.1 Effects of modifications

To ensure that the limitation of the pipe length had no effect on the characteristics of the flow through the porous pipe, simulations has been made in COMSOL[2]. This was done by assuming validity of Darcy's law, Eq. (2.18), and keeping a constant length of the pipe. The length of an open section was then varied, and the expected permeate flow rate was plotted as a function of the length. The permeate flow should be directly proportional to the length of the open section if no end-effects are present.

---

[1]Sodium hydroxide, a strong alkaline compound

[2]All calculations in COMSOL is done in the multiphysics package, assuming axial symmetry in 2D. The flow is assumed to be steady state, and the fluid incompressible.
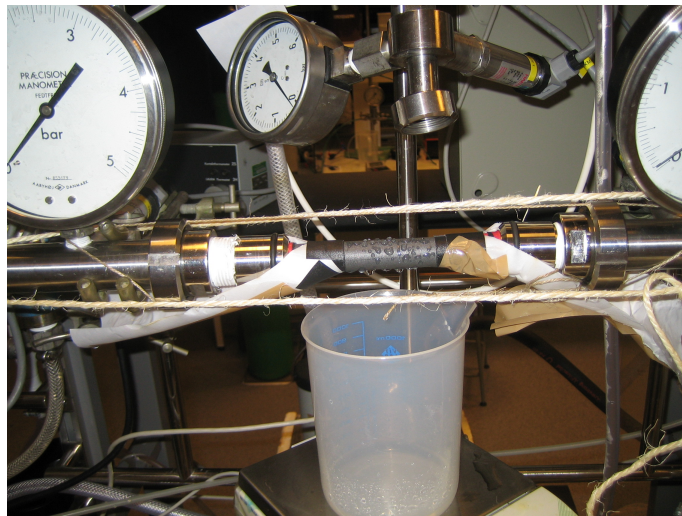
Figure 7.1: *The porous pipe in free air. The length of the pipe has been decreased using waterproof tape. The strings on the picture was necessary to hold the two manometers together, as the pressure exerted a force that repelled the two ends. As the length of the test section were shorter than the diameter of the bowl on the weight, it was necessary to mount gutters to guide the water away.*

Fig. 7.2 shows the results from COMSOL. The linearity of the graph indicates no end effects. It is therefore concluded that an open section of the pipe of a given length can be assumed to have the same characteristics as a porous pipe of same length.

7.2   Results

Again, matching values of pressure and flow rate was measured. The pressure was varied from $p_{tm} = 0.4 \times 10^5$ Pa to $p_{tm} = 4.0 \times 10^5$ Pa.

Fig. 7.3 shows the results of two series of experiments, using the same pipe. The flow rate is normalized with respect to the length, as two different lengths are tested.

The shape of the graph still indicates pre-Darcy flow, but the flow rate is reduced considerably, which points to leaks in the sealing in the experiments with the open pipe.

Possible errors due to the test setting are described in Section 4.3. The sources of error regarding the flow rate measurements are assumed to be taken into account by removing the steel housing, and by decreasing test section to avoid extra flow from the sealing.

Calibration of the manometers has also been performed for each measurements, but it has not been possible to examine if the offset of the manometers were constant when applying up to 4.0×10^5 Pa of pressure. It was also difficult to establish the influence of the pressure variations when measuring low pressures.

It was therefore decided to simplify the experimental setting to avoid the unknown factors described above. The simplified setting developed, introduced the siphon principle as the method to apply pressure.
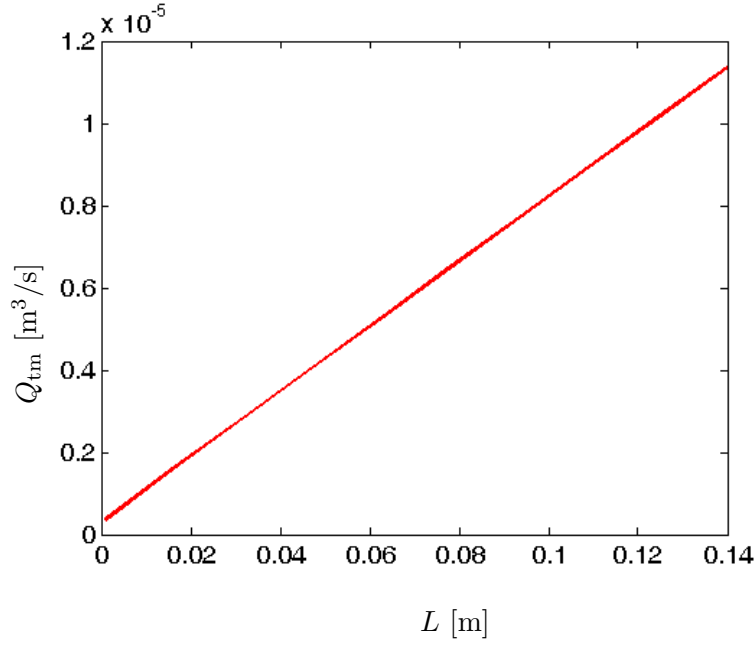
Figure 7.2: *Expected permeate flow, Q_{tm}, from the open section as a function of length L The different flow rates are calculated in COMSOL.*

7.3 Siphon experiments

The working principle of the siphon setting is described in Section 4.2.2. The advantage is the simplicity, which reduces the possible errors to human measurements with a ruler. It is assumed that the uncertainty of measuring the height of the water column is limited to 5 mm, corresponding to a pressure of

$$\Delta \mathrm{p}_{error} = \rho g h = 49 \text{ Pa}, \tag{7.1}$$

which is 1.25% of the lowest pressure measured. This should be compared with the fact that the pressure measured by the manometers in the pump setting at low pressures corresponded in size to the offset of the manometers. The results of the siphon experiments can be seen in Figs. 7.4 and 7.5 together with the results from the pump setting.

It is obvious from the figure that the two experiments can be compared, which leads to the conclusion that the results obtained by the pump setting are valid, and that the reason for pre-Darcy flow must be found elsewhere.
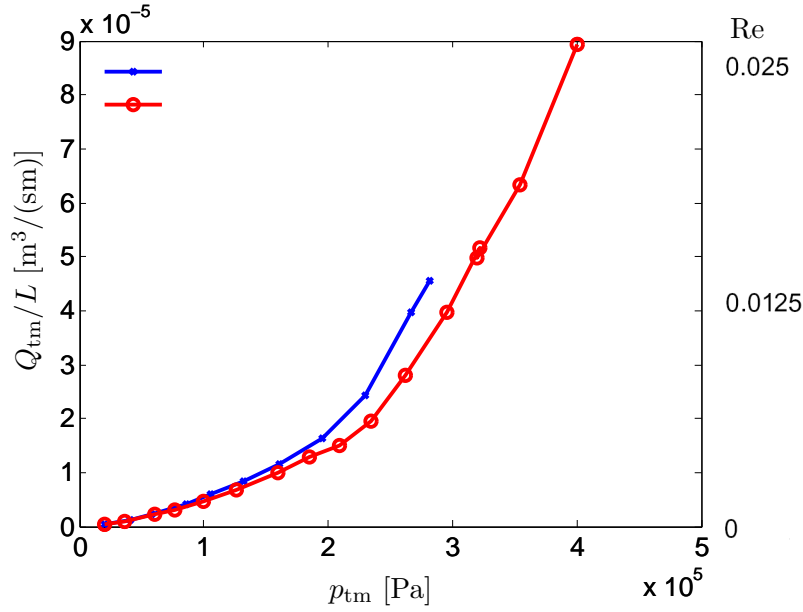
Figure 7.3: *Flow rate through pipe walls, Q_{tm}, pr. unit length as a function of pressure, p_{tm}, for different lengths of porous pipe. The two graphs are results from the same pipe, with different lengths of the open section. They were therefore expected to coincide for the normalized flow rate. The scale on the right side of the figure indicates the size of the Reynolds numbers in the flow, which are seen to be several orders of magnitudes higher that 10^{-5}*

7.4   Hysteresis

The system was tested for hysteresis, in common with the plug experiments. The measurements commenced at low pressure, increased to maximum, and then decreased again to zero.

Fig. 7.6 shows the results of the experiment. A hysteresis loop is clearly identifiable, as the graph indicates higher flow rates for pressures decreased from higher pressures. It should be noted that the hysteresis was not permanent, as the two graphs coincides at low pressures.

This behavior is emphasized in Fig. 7.7, where the measurements were interrupted at $p_{tm} = 2$ bar coming from high pressure, because of pump failure. When the measurements were continued immediately after, the hysteresis was not present.
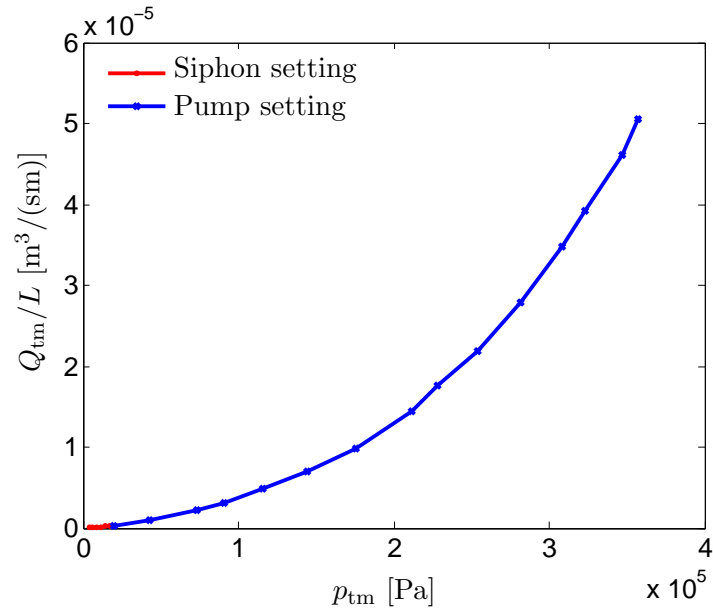
Figure 7.4: *Measured flow rate, Q_{tm}, vs. p_{tm} using the siphon setting for $0 < p < 0.2$ bar, and the pump setting for $0.2 < p < 3.5$ bar. The flow rates are normalized by length of the pipe to enable comparison of the results.*
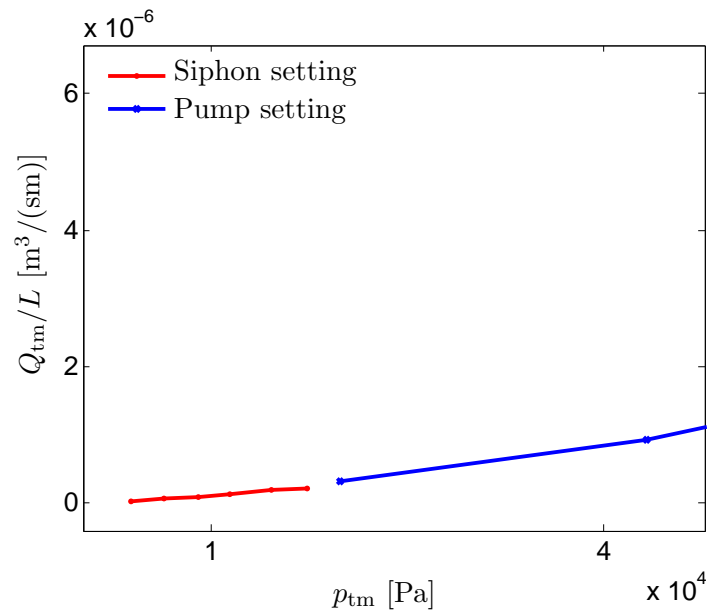
Figure 7.5: *Zoomed picture of Fig. 7.4. The results from the two methods are in accurate extension of one another, and thereby verify the results obtained using only the pump setting.*
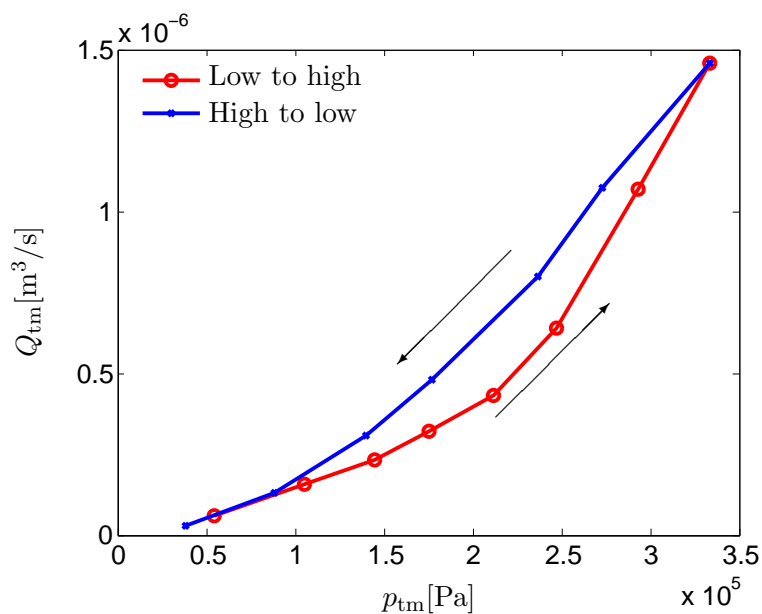
Figure 7.6: *The hysteresis effect in the porous pipe. Notice that the graph coincides at lower pressures, showing that the hysteresis is not permanent*
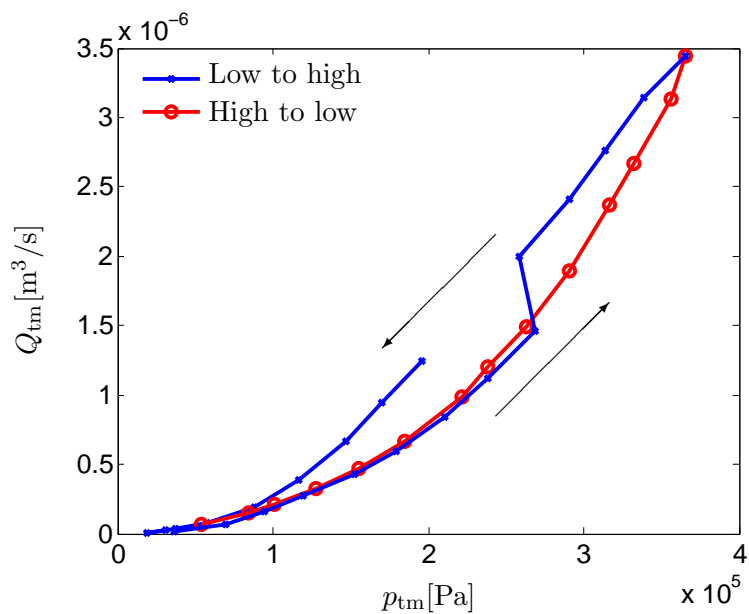
Figure 7.7: *The hysteresis effect in the porous pipe, with an interruption of measurements coming from higher pressures. Notice that the graph coincides with the graph coming from lower pressures.*

7.5 Conclusion of the blocked pipe experiments

In this series of experiments, a great effort has been put into eliminating factors, that might influence the results. Still, the results indicated pre-Darcy flow, even though the Reynolds number was greater than the limit suggested in Chapter 2.

Chapter 8

Discussion

The plug experiments indicated, as expected, that the relationship between flow rate in the porous SiC and the applied pressure gradient was linear. The variations in the measurement of the permeability has been referred to as uncertainties in the handling of the plugs, being effects from the cutting, and anisotropy in the plug, e.g. cracks. The permeabilities obtained were all in an acceptable range of the expected, which was also subject to considerable uncertainties due to the estimation of the pore sizes.

The flow in the porous pipe is found to be above proportional, meaning that the permeability of the porous SiC increases, as the pressure increased. The shape of the graphs produced resembles that of a pre-Darcy flow, which was not expected, as the limit of Re = 10^{-5} was not exceeded.

To find an explanation of the pre-Darcy flow, an extensive research of the literature was initiated. Ref. [14] argues that a Reynolds number with the permeability incorporated is a more effective way to define a demarcation parameter. This will make it comparable to a wider range of flow situations, because of the clear definition of the variables involved. It is easier to define the permeability, than to define a particle size.

Nevertheless, it was not possible to measure the permeability for the pipe, as it changed non-linearly with the pressure applied.

Ref. [17] determines a wider range of pre-Darcy flow, than the one stated by Ref. [16] which is used in this thesis. This disagreement in literature made it necessary to direct the attention to the possible explanations of above proportional flows.

8.1   Pre-Darcy flow

When Darcy's law is not applicable because of the very low rate, the flow is characterized as a pre-Darcy flow. The subject is solely treated in the area of geophysics, where Ref. [18] argues the main reason of pre-Darcy flow to be interactions with the porous medium. If the solid somehow can be dissolved in the fluid, it will change the viscosity. In the present case, were the porous medium is SiC, this effect will not be present, as porous SiC is consolidated, and not possible to dissolve in water.

Another explanation of the pre-Darcy flow is suggested by Ref. [15]: Polar water

molecules orients themselves in electric fields around surfaces. This could lead to the formation of a quasi-crystalline layer of bound water at surfaces, held in place by weak hydrogen bonds. This bound water layer could reduce the effective diameters of the pores, or even completely block them. At very low applied gradients, the hydrogen bonds would resist water movement. This could result in a threshold gradient observed at the macroscopic level. As the applied gradient increases, the bound water layer would break down, and thereby result in the above proportional relationship of the flow rate vs. the pressure gradient. However, this effect is only encountered at a scale of 10^{-9}m Ref. [21], and it is therefore not assumed to be the main explanation of the pre-Darcy flow.

Throughout the thesis, it has been assumed that a demarcation parameter between pre-Darcy and Darcy flow can be stated as the Reynolds number, using the mean particle diameter as length scale. This assumption is subject to uncertainty, as Ref. [21] claims that there is no basis for assuming Reynolds number to be determining for non-Darcy flow in a flow situation with rigid and neutral pore walls regarding the flowing liquid.

8.1.1   Saturation of water in the porous SiC

The porous SiC is said to be saturated with water if the void volume $\mathcal{V}_{void} = \phi \mathcal{V}_{\text{total}}$ is completely filled with water, i.e. $\mathcal{V}_{\text{liquid}} = \mathcal{V}_{void}$. However, it is possible that a certain volume of gas, $\mathcal{V}_{\text{gas}}$, remains entrapped in the porous medium, such that the volume containing liquid is reduced,

$$\mathcal{V}_{\text{liquid}} \;\;=\;\; \mathcal{V}_{void} - \mathcal{V}_{\text{gas}} \qquad \Rightarrow \tag{8.1}$$

$$\mathcal{V}_{\text{liquid}} \;\;=\;\; \phi \mathcal{V}_{\text{total}} - \mathcal{V}_{\text{gas}}. \tag{8.2}$$

As described in Chapter 2, an assumption for validity of Darcy's law is a fully saturated flow. Saturation of water in a porous medium is defined as

$$S_{\text{liquid}} = \frac{\mathcal{V}_{\text{liquid}}}{\mathcal{V}_{\text{void}}}, \tag{8.3}$$

In Fig. 8.1, the porous SiC walls of the pipe are seen to be hydrophilic, i.e. it has an affinity for water, as the water is attracted to the porous SiC walls. Water will therefore initially fill the small pores, as these exerts the largest capillary force on the water. As the pores vary in sizes the water will flow around the air in some pores, and thereby trap the air. Due to the nature of SiC particles, being irregular in shapes and sizes, the bubbles of air will experience a static friction called pinning.

Ref. [24] describes how surface tension on a drop of water changes as the water vaporizes, i.e. the water "pins" to the surface. In analogy to solid mechanics, this can be described as a static friction, where a certain stress needs to be applied before the subject moves. In this case the subject is an air bubble in the pores of porous SiC.

Therefore, these bubbles will only disappear if the air is dissolved in the water, or the pressure gradient is sufficient to overcome the static friction and squeeze the bubble through the small pores.

With trapped air bubbles in the porous medium, the flow rate through the medium will be decreased as the air blocks some of the pores. With increasing pressure, the bubbles
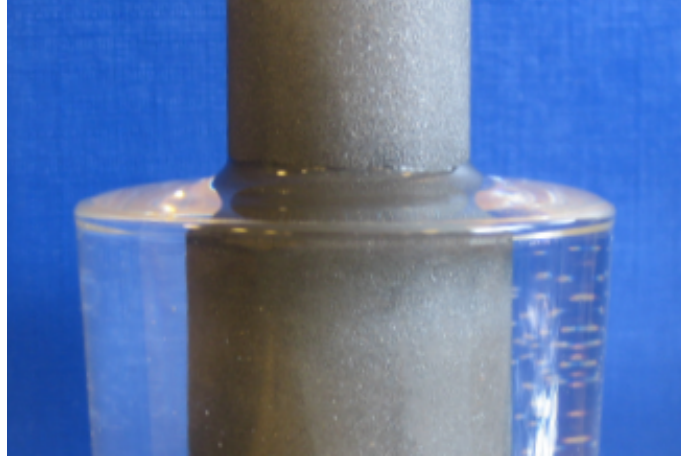
Figure 8.1: *It can be seen from the surface tension of the water that porous SiC is hydrophilic, as the water "bends upward" approaching the porous pipe*

will be compressed, and thereby increasing the permeability. This hypothesis fits well with the experimental results obtained in the open pipe and in the blocked pipe experiments, as it could explain the shape of the graphs.

Assuming a directly proportional flow rate through the porous medium to the volume of the sample, which holds for isotropic media, Ref. [1], following equation can be stated

$$\mathcal{V}_{liq} = \phi \mathcal{V}_{\text{total}} - \mathcal{V}_{\text{gas}}. \tag{8.4}$$

Neglecting thermal effects, the gas volume $\mathcal{V}_{\text{gas}}$ can be expressed by using Boyle's law as

$$\mathcal{V}_{\text{gas}} = \frac{C}{p_{\text{tm}} + 2p_{\text{perm}}}, \tag{8.5}$$

with $C = 2p_{\text{perm}}\mathcal{V}_{0,gas}$ where $\mathcal{V}_{0,gas}$ is the initial volume of the gas in the porous medium. Using Darcy's law Eq. (2.18) for the porous pipe, Eq. (8.4) can then be rewritten to

$$Q_{tm} = \frac{k}{\eta}\frac{A}{w}p_{\text{tm}} = \frac{k}{\eta}\frac{\mathcal{V}_{liq}}{w^2}p_{\text{tm}}. \tag{8.6}$$

It shall be noted that it was not possible to estimate the volume of the gas trapped in the porous medium at atmospheric pressure. This equation is stated to qualitative validate the assumption of saturation being the explanation of the above proportional behavior of the results. An example of the shape of the graph is seen in Fig. 8.2, which show, that compression of the gas in the porous media can explain the shape of the results obtained The graph should only be viewed as purely qualitative, as there are several factors which influence on the calculations, e.g. the initial amount of gas in the pipe and the estimation of the permeability.

It could be argued that the porous pipe would be saturated if the experimental setup was given enough time to dissolve the air. The measuring time was 60 s in the measure-
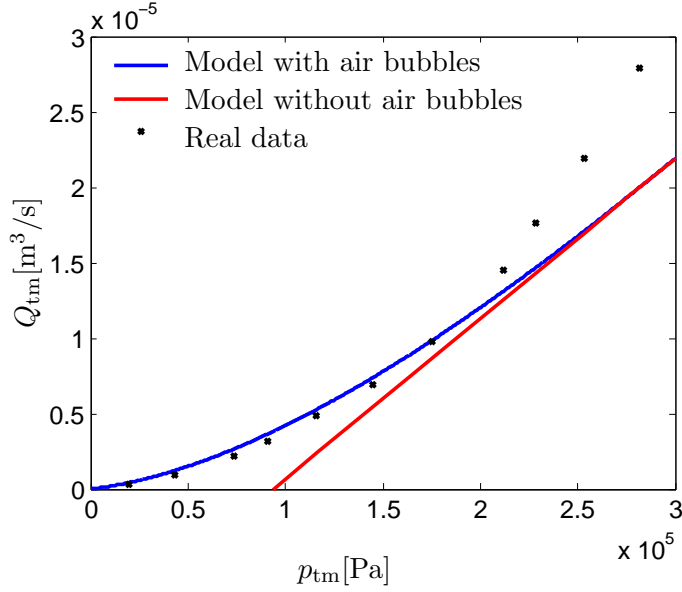
Figure 8.2: *The expected shape of the flow rate through the porous wall as a function of pressure, assuming air being compressed in the pores. The parameters used to calculate the graph is taken from Section 2.2.4.*

ments, and it was assumed that the system was steady. Fig. 8.3 shows a graph of the mass flux, which appears to be constant.

The trapped air bubbles in the porous SiC can disappear by dissolving in the water. Depending on the fluid velocity, and the initial level of gas saturation in the fluid, this may take considerable longer time than the measuring time in the experiments conducted in this thesis work.

The amount of air that can be dissolved in water per time depends on the amount already dissolved in the water, and by the partial pressures of the individual gases in air, mainly nitrogen ($\approx 79\%$) and oxygen ($\approx 21\%$). According to Ref. [6], Henry's law states that the concentration of a gas dissolved in a liquid is equal to the partial pressure of the gas over the liquid times the solubility coefficient of the gas. Therefore, the air will be removed more rapidly at high pressures than low pressures.

The velocity in a porous medium can be defined in two different ways: The mean velocity of the fluid pr. surface area of the medium is called the macroscopic velocity, v_{mac}. The microscopic velocity, v_{mic}, is the actual velocity in the pores, and is defined by

$$v_{mic} = \frac{1}{\phi\sqrt{\tau}} v_{mac} \qquad (8.7)$$
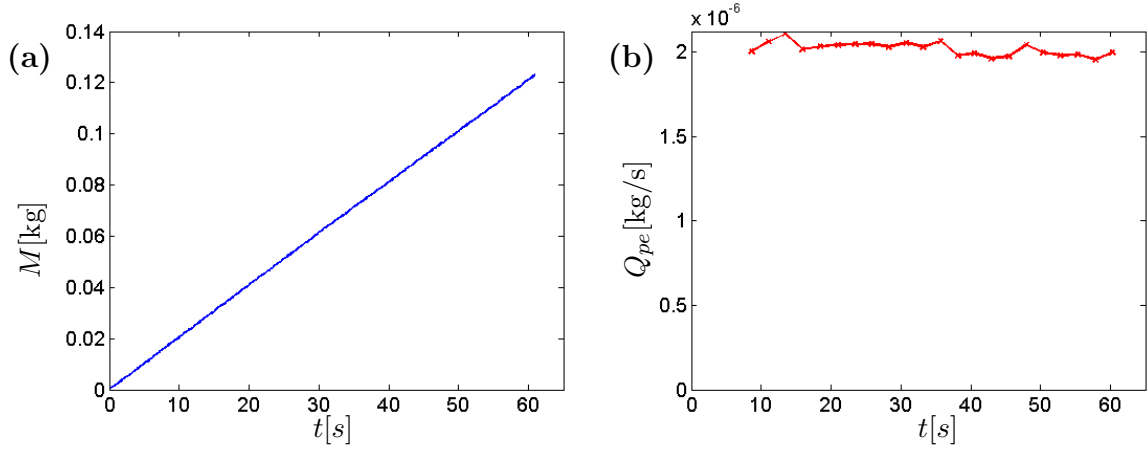
Figure 8.3: *(a) shows the weight as a function of time at constant p_{tm}.(b) shows the mass flux as a function of time at constant p_{tm}. The data of the mass flux has been divided into bins of 2 s, and then averaged. Using this method makes the data easier to interpret, as it eliminates the worst fluctuations*

by using continuity. It is seen that v_{mic} depends on the porosity and the tortuosity of a porous medium. The amount of air removed will depend on the microscopic velocity, as only a certain amount of air can be dissolved in a given volume of water. A higher flow rate will therefore result in more air removed as a larger volume of water will be able to dissolve the air.

It is difficult to anticipate the time for removing all of the air present in the porous pipe, as the amount of air is unknown. Unto that must be added that the initial saturation of air in the water is also unknown. Nevertheless, it can be concluded that the time scale probably is exceedingly higher than the measuring time used in the experiments, as a constant flow rate was observed, see Fig. 8.3.

The plug experiments did not demonstrate the same behavior as the porous pipe, which leads to the conclusion that the solid matrix in the plugs had different characteristics in order to prevent air bubbles from being trapped. From the SEM-pictures in Fig. 4.9 in Chapter 6, one difference could be a fundamental different particle size distribution, as a large amount of small particles are observed, compared to the other picture of a standard carrier.

8.1.2   Hysteresis

As seen on Fig. 7.6, a hysteresis loop was identified when the results were plotted. The initial thought was that the hysteresis was due to the experimental setup. However, the plug experiments showed, that the experimental setup was able to show linearity in the plug experiments, an that no hysteresis was present.

If the reason for the pre-Darcy behavior of the flow can be explained by the trapped air in the pores, it is argued that this might also be the explanation of the hysteresis observed.

The pinning of the air bubbles, as described in the previous section, will also come into consideration when the gas bubbles expands for pressures going from high values to low

The capillary pressure in the pores are also subject to hysteresis, as the contact angle is a function of direction of the displacement. This effect is referred to as the raindrop effect, and can, again in analogy with solid mechanics, be described as kinematic friction. The kinematic friction is in this case higher for air displacing the water, than for water displacing the air, which implies hysteresis.

8.2   Experiments to be conducted

Given the resulting data obtained during the thesis work, it is clear that further experimental investigations are needed to fully understand the flow in porous SiC.

The focus of the suggested experiments is concentrated on more precisely determining the the reason of the pre-Darcy behavior of the flow in this porous SiC pipe. As mentioned in the previous section, the measuring time in the blocked pipe might not be sufficient to saturate the porous pipe. It is therefor suggested to conduct experiments with longer measuring time, to see if the flow rate changes for constant pressure.

The pipe experiments should be repeated with other porous pipes, of different dimensions, to determine if the pre-Darcy behavior is a common phenomenon in porous pipes, or this was a special case.

8.2.1   Influence of gas

The volume of the gas is dependent on the total pressure and the volume flow is only dependent on the trans membrane pressure. By designing a test setting, where the pressure on the permeate side can be controlled, it will be possible to increase the total pressure, and keeping the trans membrane pressure constant. Darcy's law states that the flow rate in a porous medium is only dependent on the pressure difference for constant material properties. Therefore, if Darcy's law is valid, the flow rate should be constant when increasing the total pressure.

By conducting these experiments, it will be possible to determine if lack of saturation is the reason for the above proportionality in the results of the porous pipe experiments in Chapters 6 and 7.

8.2.2   Bubble point

To get an idea of the isotropy of the porous SiC, a simple technique would be to measure the bubble pressure of the sample, Ref. [20]. The bubble pressure is defined as the pressure needed to blow air through a liquid filled porous sample, and is measured by immersing a porous sample in water. Air under pressure is applied to one end, and the air pressure is gradually increased. When the pressure reaches a certain level, bubbles of air will penetrate the membrane. This pressure is called the bubble pressure. By assuming spherical particles

in the medium, the maximum pore size can be determined by

$$r_{\text{pore, max}} = 2\cos(\theta)\frac{\gamma}{\Delta p_{\text{bubble}}} \tag{8.8}$$

where $r_{\text{pore, max}}$ is the maximal pore size of the porous medium, θ the contact angle between the porous material and the fluid, γ is the surface tension at the liquid air interface and finally Δp_{bubble} the pressure difference.

If the pressure is increased beyond the bubble pressure, the air will penetrate the smaller pores. If the bubbles are evenly distributed on the surface of the porous medium, it can be assumed to be isotropic.

8.2.3 Porosity measurement

Ref. [2] suggests several methods to determine the porosity in a porous sample. In this project, the total porosity of the porous pipe was estimated by weighing the sample, and compare it with a solid sample. The disadvantage of this method is that it measures the total porosity, i.e. the "blind" pores are also taken into account, even though these does not contribute to the volume of the conducting pores.

A way to determine the effective porosity is the gas expansion method. The sample is enclosed in a container of known volume, under known gas pressure, and is connected with an evacuated container of known volume. When the two containers are connected, the gas pressure will decrease due to the increased volume.

The effective pore volume can then be calculated by

$$\mathcal{V}_p = \mathcal{V}_{\text{total}} - \mathcal{V}_a - \frac{p_2}{p_2 - p_1}\mathcal{V}_b, \tag{8.9}$$

deduced from the ideal gas law, $pV = nRT$. $\mathcal{V}_a$ is the volume of the container with the sample, $\mathcal{V}_b$ is the volume of the evacuated container, $\mathcal{V}_{\text{total}}$ volume of the porous sample, p_1 the initial pressure, and p_2 the final pressure.

From the pore volume the effective porosity can be calculated.

Chapter 9

Conclusion and outlook

This thesis work was initiated with the ambition of creating a model for flow in porous SiC, which would be able to assist in the construction and the design of SiC-membranes.

The governing equations have been stated, and it has been shown analytically, that the flow in porous SiC should follow Darcy's law, i.e. the flow rate should be proportional with the pressure gradient applied.

In order to validate the calculations and assumptions, simple experiments were designed and performed. It was shown, that Darcy's law is applicable in porous SiC for Re = 0.2. However, it was also found, that Darcy's law was not applicable in the porous pipe flow experiments.

It was argued, that lack of saturation was the reason for this deviation. This appeared to be a very complicated process, as the determining parameters are difficult to obtain. The fact that the plug experiments obeyed Darcy's law, and the pipe experiments failed was subject to wonder, as they appeared to have the same characteristics, i.e. same particle size and porosity. The lack of saturation must therefore be very dependent properties of the solid matrix, which has not been possible to estimate in this investigation, being the tortuosity and the particle size distribution.

Due to this unexpected complexity of creating a full model of the flow in porous, this was not completed in this thesis. Nevertheless, the thorough investigation of the flow has revealed characteristics of SiC, which is important to know in order to create such a model. The ground is thereby laid for further investigation.

9.1 Outlook

The fact, that pre-Darcy flow can occur in porous SiC-membranes should be subject to a thorough investigation, as it is determining for the properties in porous SiC membranes. This thesis work has laid the ground for further investigation of the flow, in order to determine a full model of the flow.

9.1.1   Square channels in a membrane carrier

A membrane carrier can feature from one to several hundreds channels which exists in various forms, with the most used being circular and square. A typical carrier design is seen in Fig. 9.1.
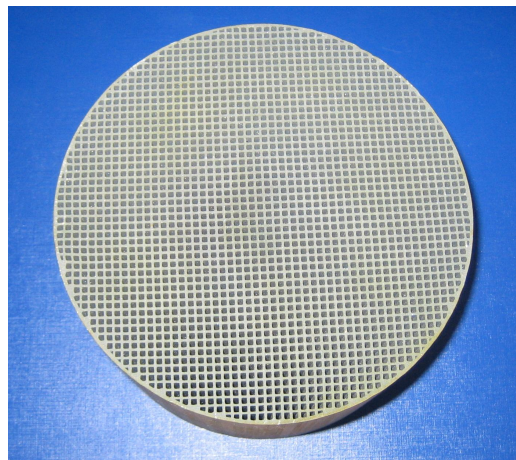
Figure 9.1: *A standard multiple channel porous SiC carrier from CoMeTas A/S. The carrier has a diameter of 144 mm with 2mm × 2mm channels.*

In the field of membranes, the capacity of a given membrane is measured by the area of the membrane layer. The design of a carrier, similar to the one in Fig. 9.1 has been chosen in order to increase the area of the membrane layer on the walls of the open channels.

Once a full model of the flow in porous SiC can then used to determine the actual flow in the carrier, as every channel might not filter the same amount of fluid.

This would be of great interest from a commercial viewpoint, as the design of the carrier most likely can be optimized, not only for maximum membrane area, but for maximum effective membrane area.

9.2   Relation of obtained results to membrane technology

The focus of the thesis has been to relate the discovered properties of the flow in porous SiC to a commercial view point, as it may improve the design of ceramic cross-flow membrane in the future.

The fact that air can be trapped in the pores, and in some cases can be extremely complicated to remove, will have to be considered, when an estimate of the flow rate through a membrane is made.

The practical significance of this will be, that it in some cases, depending on the fluid and pore size of the porous medium, will be necessary to initiate the flow at a higher trans membrane pressure than the working pressure desired. Due to the hysteresis observed, this procedure could increase the flow in the membrane.

Appendix A

Appendices

A.1   Extrusion

UNLESS OTHERWISE SPECIFIED:

DIMENSIONS ARE IN MM
TOLERANCES:
FRACTIONAL ±
ANGULAR: MACH ±   BEND ±
TWO PLACE DECIMAL ±
THREE PLACE DECIMAL ±

INTERPRET GEOMETRIC
TOLERANCING PER:

MATERIAL: Plast

FINISH

DO NOT SCALE DRAWING

	NAME	DATE
DRAWN	TEH	31/10-2006
CHECKED		
ENG APPR.		
MFG APPR.		
Q.A.		
COMMENTS:		

Tlf. 2514 2195

Thomas Eilkær Hansen

TITLE:

Plast til ekstruderhovede

SIZE **A** | DWG. NO. | drawing | REV
SCALE: 1:1 | WEIGHT: | SHEET 1 OF 1

NEXT ASSY | USED ON

APPLICATION

$\varnothing 15 ^{+0.25}_{-0.25}$

$\varnothing 8.50 ^{+0.50}_{0}$

$100 ^{+2}_{-2}$

$7 ^{+1}_{-1}$

$11 ^{+1}_{-1}$

A.2   MatLab code

A.2.1   Example of MatLab script for sorting data in the plug experiments

```
close all, clear all, clc
%%%%%%%%%%%%%%%%%%%%%%%%%%%%%%%%%%%%%%%%%%%%%%%%%
% Script to process data from the plug experiments
%%%%%%%%%%%%%%%%%%%%%%%%%%%%%%%%%%%%%%%%%%%%%%%%%

%Flow constants:
phi = .45;
dm  = 12e-6;                    % Mean particle diameter    [m]
g   = 9.82;                     % Gravitation               [m/s^2]
nu  = 1e-6;                     % Kinematic viscosity       [m^2/s]
R   = (23.4/2)*1e-3;           % Radius of plug            [m]
A   = pi*R^2;                   % Area of plug              [m^2]
eta = 1e-3;                     % Dynamic viscosity         [Pa s]
rho = 1e3;                      % Density                   [kg/m^3]


k   = dm.^2*n^3/(180*(1-n)^2)   % Permeability calculated using Kozeny Carman [m^2]

L   = 22.45e-3;                 % Length of plug            [m]
dP  = linspace(1e4,4e5,np)/L;
oop = 1;

v0  = k/eta*dP;                 % maximum velocity
Q = v0*A;

% Pressure calibration constants:
pkout = -16103.068;
pkin  = -1599.9396;
pkperm= -8535.5736;
%%%%%%%%%%%%%%%%%%%%%%%%%%%%%%%%%%%%%%%%%%%
%% EXPERIMENTS
%%%%%%%%%%%%%%%%%%%%%%%%%%%%%%%%%%%%%%%%%%%

dname = dir('data2310/d2310n*');
names = struct2cell(dname);
names = names';
wn = 0;
cd data2310
% Number of files
nv = [1:9];

drb = 10;       % Data range limiter, beginning
dre = 10;       % Data range limiter, end

for n = 1:length(nv)
    name = nv(n);
    str = char(names(name));
    [labels t data] = readcoldata(str,5,7,1);

    %%%%%%%%%%%%%%%%%%%%%%%%%%%%%%%%%%%%%%%%%%%%%%%%%%%
    % Sorting data:
    %%%%%%%%%%%%%%%%%%%%%%%%%%%%%%%%%%%%%%%%%%%%%%%%%%%
    srti = find(abs(data(:,3) - mean(data(:,3))) > 4e-1);
    data(srti,:) = [];

    srto = find(abs(data(:,2) - mean(data(:,2))) > 4e-1);
    data(srto,:) = [];
```

```matlab
%%%%%%%%%%%%%%%%%%%%%%%%%%%%%%%%%%%%%%%%%%%%%%%%%%%%%%%%%%
wedr   = data(drb:end-dre,1)*1e-3;
pindr  = data(drb:end-dre,3)*1e5;
poutdr = data(drb:end-dre,2)*1e5;
tdr    = t(drb:end-dre);

% Binning of the data
sob = 10;             % Size of bins
nn = 1:sob:floor(length(wedr)/sob)*sob;

for j = 1:length(nn)-1
    wed(j)   = mean(wedr(nn(j):nn(j+1)));
    td(j)    = mean(tdr(nn(j):nn(j+1)));
    pind(j)  = mean(pindr(nn(j):nn(j+1)));
    poutd(j) = mean(poutdr(nn(j):nn(j+1)));
end


pinv(n)  = mean(pind)- pkin;
poutv(n) = mean(poutd)- pkout;

Mf       = ((wed(end)-wed(1))./(td(end)-td(1))); % Mass flow [kg/s]
Qpe(n)   = mean(Mf/rho);                         % Volume flow, [m^3/s]
    clear dpe Qe pind poutd dpen Qendata wed td
end

tmp    = pinv-poutv;
cd ..

coeffm = polyfit(tmp/L,Qpe,1);

kem = coeffm(1)*eta/A;
krou = round(kem*1e14)/1e14;
%%%%%%%%%%%%%%%%%%%%%%%%%%%%%%%%%%%%%%%%%%%%%%%%%%%%%
% Plotting:
%%%%%%%%%%%%%%%%%%%%%%%%%%%%%%%%%%%%%%%%%%%%%%%%%%%%%
figure(n+1)
axes('fontsize',14)
plot(tmp,Qpe,'r-o','linewidth',2)
title(['Plot for plug 6, L = ' num2str(L) 'm, k = ' num2str(krou)])
legend('p_{in}','p_{out}','p_{perm}','Location','NorthWest')
xlabel('pressure [Pa]'), ylabel('Q_{pe} [m^3/s]')
```

A.2.2 Example of MatLab script for sorting data in the pipe experiments

```
close all, clear all, clc
%%%%%%%%%%%%%%%%%%%%%%%%%%%%%%%%%%%%%%%%%%%%%%%%%%%
% Script to process data from the pipe experiments
%%%%%%%%%%%%%%%%%%%%%%%%%%%%%%%%%%%%%%%%%%%%%%%%%%%

%Flow constants:
phi = .45;
dm  = 12e-6;                    % Mean particle diameter    [m]
g   = 9.82;                     % Gravitation               [m/s^2]
nu  = 1e-6;                     % Kinematic viscosity       [m^2/s]
r   = 20/2*1e-3;               % Radius of pipe            [m]
A   = 2*pi*r*L;                % Area of plug              [m^2]
eta = 1e-3;                     % Dynamic viscosity         [Pa s]
rho = 1e3;                      % Density                   [kg/m^3]
L   = 0.124;                    % Length of pipe
k   = dm.^2*n^3/(180*(1-n)^2)  % Permeability calculated using Kozeny Carman [m^2]
v0  = k/eta*dP;                 % maximum velocity
w   = 3.5e-3;                   % Wall thickness
2*pi*r*L;
allf= 0;


nox = 1e2;


% Pressure calibration constants:
pkout =  -16103.068;
pkin  =  -1599.9396;
pkperm=  -8535.5736;


dname = dir('data2201/d2201*');
names = struct2cell(dname);
names = names';
wn = 0;
cd data2201


% a:
nv = [1:4 6:8]; Qplot = [];
%nv = 4
h = [1.68 2.12 0.93 1.16 0.565 1.565 1.75];
p = rho*g*h;

% All:
%nv = [1:12 13:27 27:41], allf = 1; Qplot = [3.6e-5 4.8e-5 6.0e-5]

%nv = [1];
drb = 20;        % Data range limiter, beginning
dre = 5 ;        % Data range limiter, end

for n = 1:length(nv)
    name = nv(n);
    str = char(names(name));
    [labels t data] = readcoldata(str,5,7,1);

    %%%%%%%%%%%%%%%%%%%%%%%%%%%%%%%%%%%%%%%%%%%%%%%%%%%%
    % Sorting data:
    %%%%%%%%%%%%%%%%%%%%%%%%%%%%%%%%%%%%%%%%%%%%%%%%%%%
    srti = find(abs(data(:,3) - mean(data(:,3))) > 4e-1);
    data(srti,:) = [];
```

```matlab
    srto = find(abs(data(:,2) - mean(data(:,2))) > 4e-1);
    data(srto,:) = [];

    %%%%%%%%%%%%%%%%%%%%%%%%%%%%%%%%%%%%%%%%%%%%%%%%
    wedr   = data(drb:end-dre,1)*1e-3;
    pindr  = data(drb:end-dre,3)*1e5;
    poutdr = data(drb:end-dre,2)*1e5;
    tdr    = t(drb:end-dre);

    % Binning of the data
    sob = 10;              % Size of bins
    nn = 1:sob:floor(length(wedr)/sob)*sob;

    for j = 1:length(nn)-1
        wed(j)  = mean(wedr(nn(j):nn(j+1)));
        td(j)   = mean(tdr(nn(j):nn(j+1)));
        pind(j) = mean(pindr(nn(j):nn(j+1)));
        poutd(j) = mean(poutdr(nn(j):nn(j+1)));
    end


    pinv(n)  = mean(pind)- pkin;
    poutv(n) = mean(poutd)- pkout;

    Mf       = ((wed(end)-wed(1))./(td(end)-td(1))); % Mass flow [kg/s]
    Qpe(n)   = mean(Mf/rho);                         % Volume flow, [m^3/s]
    clear dpe Qe pind poutd dpen Qendata wed td
end
tmps = sort(tmp);
Qpes = sort(Qpe);

%%%%%%%%%%%%%%%%%%%%%%%%%%%%%%%%%%%%%%%%%%%%%%%%%%
% Reynold's numbers:
%%%%%%%%%%%%%%%%%%%%%%%%%%%%%%%%%%%%%%%%%%%%%%%%%%

% Entrance to porous pipe:
Re_ent = 2*rho*Qpes./(pi*r*eta)

% At manometer:
d_man = 8e-3;
Re_man = 4*rho*Qpes./(pi*d_man*eta)

% In the porous SiC:
Re_sic = rho*Qpes*npo*dm/(2*eta*r*pi*L)

%%%%%%%%%%%%%%%%%%%%%%%%%%%%%%%%%%%%%%%%%%%%%%%%%%%
% Plotting
%%%%%%%%%%%%%%%%%%%%%%%%%%%%%%%%%%%%%%%%%%%%%%%%%%%
figure(n+1)
axes('fontsize',14)
plot(tmp,Qpe,'r-o','linewidth',2)
title(['Plot for Q_e = ' num2str(Qplot) 'm^3/s'])
legend('p_{in}','p_{out}','Location','NorthWest')
xlabel('tmp [Pa]'), ylabel('Q_{pe} [m^3/s]')
```

Bibliography

[1] *Dynamics of fluids in porous media*
     Jacob Bear
     American Elsevier Publishing Company (New York, 1972)

[2] *Porous Media, Fluid Transport and Pore Structure*
     F. A. L. Dullien
     Academic Press, Inc. (New York, 1979)

[3] *Theoretical microfluidics*
     Henrik Bruus
     2006, MIC - Department of Micro and Nanotechnology www.mic.dtu.dk/bruus

[4] *Mechanics of heterogeneous fluids in porous media*
     Arthur T. Corey
     Water Resources Publications (Fort Collins, Colo. 1977)

[5] *Viscous Fluid Flow*
     Frank M. White
     McGraw-Hill Book Co., (Singapore, 1991)

[6] *Statistical Physics*
     Landon & Lifshitz, vol. 5
     Butterworth & Heinemann (Oxford, 2001)

[7] *Fundamentals of Inorganic Membrane Science and Technology*
     Edited by:
     A. J. Burggraf and L. Cot
     Elsevier Science B. V. (Amsterdam, 1996)

[8] Webpage of CoMeTas A/S:
     www.cometas.dk

[9] Webpage of Lenntech A/S:
     www.lenntech.dk

[10] Webpage of COMSOL:
      www.comsol.com

[11] Webpage of Liqtech A/S:
      www.liqtech.dk

[12] *Flow in Porous Media I: A Theoretical Derivation of Darcy's Law*
      Journal Transport in Porous Media
      Publisher Springer Netherlands
      Issue Volume 1, Number 1 / March, 1986
      Pages 3-25

[13] Liu, S., and Masliyah, J.H.
      Single fluid flow in porous media
      Chemical engineering communications (Chem. eng. commun.), 1996, vol. 148-50, pp. 653-732 (5 p.1/2)

[14] Zhengwen Zeng and Reid Grigg
      A Criterion for Non-Darcy Flow in Porous Media
      Transport in Porous Media, Volume 63, Number 1, April 2006

[15] *Theory of Ground Water Movement*, Moscow (1952)
      Polubarinova-Kochina, P. Ya: Reprinted in English translation by J. M. R. De Wiest, Princeton University
      Press, Princeton NJ (1962) p. 17.

[16] Fand, R. M., Kim, B. Y. K., Lam, A. C. C., and Phan, R. T.
      *Resistance to the Flow if Fluids Through Simple and Complex Porous Media Whose Matrices Are Composed
      of Randomly Packed Spheres*
      ASME J. Fluids Eng., vol. 109, pp. 268-274, 1987

[17] Ifiyenia Kececioglu, Yuxiang Jiang
      Flow Through Porous Media of Packed Spheres Saturated With Water
      Department of Mechanical Engineering,
      The University of Illinois at Chicago

[18] Dale Schwartzendruber
      Non-Darcy Flow Behaviour in Liquid-Saturated Porous Media
      Journal of Geophysical Research, vol. 67, no. 13, December 1962

[19] *small rock samples using Image Analysis techniques*
      Theodoor Wouter Fens
      2000, Delft University Press, Stevinweg 1, 2628 CN, Delft, the Netherlands.

[20] Membrane Filtration
      and related molecular separation technologies.
      APV System, (Silkeborg, 2000)
      Editor: Werner Kofod Nielsen

[21] Private communication
      Alexander Shapiro
      Technical University of Denmark
      Department of Chemical Engineering
      e-mail: ash@kt.dtu.dk

[22] Private communication
      Søren Beier
      Technical University of Denmark
      Department of Chemical Engineering
      e-mail: spb@kt.dtu.dk

[23] Private communication
      Jens Nørkær Sørensen
      Technical University of Denmark
      Department of Mechanical Engineering
      e-mail: jns@mek.dtu.dk

[24] Report in course 10030, DTU, 11. december 2006 Hold 5: af s062084 Mathias Brinch-Larsen s062105 Karl
      Elkjær s052944 Mikkel Settnes s062119 Christoffer Mølleskov Pedersen